Economic Geology, v. 104, pp. 205–221

Cumulate Origin and Polybaric Crystallization of Fe-Ti Oxide Ores in the Suwalki Anorthosite, Northeastern Poland

Bernard Charlier,† Olivier Namur, Jean-Clair Duchesne,
Department of Geology, University of Liège, 4000 Sart Tilman, Belgium

Janina Wiszniewska, Antoni Parecki,
Polish Geological Institute, ul. Rakowiecka 4, 00-975 Warszawa, Poland

and Jacqueline Vander Auwera
Department of Geology, University of Liège, 4000 Sart Tilman, Belgium

Abstract

Fe-Ti oxide ores in the Proterozoic Suwalki massif-type anorthosite, northeastern Poland, have been recognized through geophysical exploration and extensive drilling down to 2,600 m depth. The Fe-Ti oxide-rich rocks from Suwalki consist of vanadium-poor Ti-magnetite in lenses varying from the centimeter- to the kilometer-scale. Fe-Ti–rich rocks are commonly layered and have gradational contacts with the host anorthosite; they do not represent well-defined intrusions such as the major Tellnes and Lac Tio deposits. Based on petrography, modal proportions, whole-rock analyses, and liquidus phase compositions of Fe-Ti oxide ores, the sequence of crystallization is as follows: plagioclase + Ti magnetite + ilmenite, followed by orthopyroxene, then clinopyroxene, and finally apatite. The comparatively low V content (0.20–0.67 wt % V) in Ti magnetite results from relatively oxidized crystallization conditions. The diapiric emplacement of the anorthositic pluton influenced the crystallization of the Fe-Ti ores and is responsible for the crystal sorting controlled by the density contrast of liquidus phases. Polybaric crystallization of Fe-Ti oxide ores is evidenced by variable Al_2O_3 (ca. 1–5 wt %) content of the associated orthopyroxene. Polybarism is responsible for the appearance of Fe-Ti oxides before orthopyroxene, due to the decreasing stability field of orthopyroxene with pressure.

Introduction

Magnetite-ilmenite ores were drilled in the early 1960s in northeastern Poland following gravimetric and magnetic surveys covering the Polish area of the East European platform and, based on additional exploration, an iron ore mine was planned during the 1970s, although this plan was not put into action. Numerous deep boreholes (down to 2,600 m depth) from this exploration activity provide a unique opportunity to better understand the Polish crystalline basement, which is covered by a thick suite of sedimentary rocks. The Fe-Ti oxide ores associated with the Suwalki anorthosite, which is part of the Mazury complex in the East European craton (Baginski et al., 2001; Wiszniewska et al., 2002; Skridlaite et al., 2003), were studied to better understand the petrogenesis of these genetically controversial deposits.

Unlike the two hard-rock deposits in anorthosites presently exploited, the Lac Tio mine, Quebec (Lister, 1966), and the Tellnes deposit, Norway (Charlier et al., 2006, 2007), which have hemo-ilmenite as the ore mineral, the Suwalki ore is dominated by vanadium-poor Ti-magnetite accompanied by ilmenite and a variable proportion of plagioclase ± orthopyroxene ± clinopyroxene ± apatite. The orebodies occur as irregular lenses or pods with gradational relations with the host anorthosite with which they are closely related. These ores do not crop out and have only been intersected by core from deep drilling at 820- to 2,600-m depth.

Segregation of an immiscible Fe-Ti-(P)–rich melt has been invoked for the formation of these ores (Speczik et al., 1988), a common interpretation for the petrogenesis of Fe-Ti-(P) deposits (Bateman, 1951; Lister, 1966; Philpotts, 1967; Kolker, 1982; Force, 1991; Zhou et al., 2005). However, other studies of Fe-Ti oxide ores have emphasized the role of fractional crystallization with Fe-Ti oxides as early liquidus phases (Duchesne, 1999; Charlier et al., 2006, 2007, 2008; Pang et al., 2008a, b). In this scenario, crystal sorting is the main mechanism for ilmenite and magnetite enrichment. Magma mixing that produced a hybrid liquid composition located in the stability field of Fe-Ti oxides has also been suggested (Robinson et al., 2003).

The magnetite-rich rocks from the Suwalki anorthosite thus constitute an important opportunity to study the Fe-Ti ore-forming processes and the controlling factors on ore composition. Fe-Ti enriched rocks sampled by cores drilled in several orebodies in the anorthosite have been used to determine whether cumulate processes, immiscibility, or alternative processes are responsible for the formation of these Fe-Ti ores. In addition, the authors explore, in this study, the role of oxygen fugacity on the incorporation of V by magnetite and the influence of the polybaric crystallization model of Proterozoic massif-type anorthosite (e.g., Emslie, 1980; Ashwal, 1993; Longhi et al., 1993) on the mechanisms of formation of Fe-Ti oxide ores.

Geologic Setting

The Mazury anorthosite-mangerite-charnockite-(rapakivi) granite suite and the Suwalki massif-type anorthosite

The Suwalki massif-type anorthosite (northeastern Poland) was discovered in 1957 as the result of a drilling campaign

† Corresponding author: e-mail, b.charlier@ulg.ac.be

carried out in order to check out gravity and magnetic anomalies identified in the early 1950s (Ciesla and Wybraniec, 1998; Ryka and Podemski, 1998). The Suwalki, Sejny, and Ketrzyn massifs together with associated granites of the Mazury complex (Fig. 1) constitute a typical anorthosite-mangerite-charnockite-(rapakivi) granite suite (Wiszniewska et al., 2002; Skridlaite et al., 2003). This suite is situated in the western part of the East European craton (Bogdanova et al., 2001; Claesson et al., 2001; Bogdanova et al., 2008) and has been dated at ca. 1.5 Ga (Dörr et al., 2002). It extends along parallel 54° from the Bay of Gdansk in the west to southern Lithuania (Skridlaite et al., 2007) and western Belarus in the east.

The top of the Suwalki anorthosite was eroded by deep peneplanation and is now buried under 580 to 1,200 m of Phanerozoic cover dipping to the southwest. The Suwalki anorthosite covers 250 km^2 of the 8000 km^2 of the Mazury complex. The pluton has an elliptic morphology ca. 30 km long by 15 km wide and a domical shape in cross section (Fig. 2). Detailed petrographic investigations by Juskowiak (1998) of 45 boreholes, located primarily in the Krzemianka and Udryn areas, gave the following relative proportion of rocks: 43 percent andesine anorthosite, 8 percent norite, 19 percent gabbronorite, 20 percent (quartz- and monzo-) ferrodiorite, 5 percent Fe-Ti oxide ore, and 5 percent granitoid. Spatially, anorthositic rocks occur in the central part whereas (quartz- and monzo-) ferrodiorites occur in the upper margins. Ferrodiorites commonly overlie gabbronorites and do not have contacts with norites and anorthosites. Gabbronorites lie in contact with norites and anorthosites and are present in boreholes located in marginal parts. However, because the Suwalki anorthosite has essentially been drilled where significant magnetic and gravimetric anomalies occur, it is most probable that other portions of the Suwalki massif are dominated by anorthosites with minor (gabbro-)norites.

Geology of Fe-Ti oxide ore bodies

Several Fe-Ti oxide ore deposits (Krzemianka, Udryn, Jeleniewo, and Jezioro Okragle; Fig. 2) were first recognized by distinct gravity and magnetic anomalies (Ciesla and Wybraniec, 1998). Krzemianka and Udryn deposits were sampled by drilling in 1962 and further exploration was concentrated in those areas (Podemski, 1998). Jezioro Okragle and Krzemianka have been dated at 1559 ± 37 Ma, which is similar to the age of Udryn at 1556 ± 94 Ma (Re-Os isochrons on magnetite and sulfides; Morgan et al., 2000).

In the Krzemianka area, 73 boreholes were drilled (total length of 135.5 km) to the depth of between 1,200 and 2,800 m. One Gt of ore has been proved, averaging 27 percent Fe, 7 percent TiO_2 and 0.3 percent V_2O_5 (Parecki, 1998), covered by ca. 900 m of Phanerozoic sedimentary rocks. The documented part of the deposit has the shape of an arch (Parecki, 1998) with a maximum width of 1.5 and length of 4.5 km. Orebodies mainly have the morphology of lenses and layers varying from a few centimeters to 145 m thick. In the Udryn area, situated in the central part of the Suwalki anorthosite, 12 boreholes were drilled to the depth of 1,200 to 2,300 m. The total length of drilling is 22.8 km. 250 Mt of ore have been proved, with similar composition to that of Krzemianka. Some minor occurrences of ore have also been located in the vicinity of Jezioro Okragle and Jeleniewo.

There are many individual orebodies with morphologies of lenses, veins, or layers. Fe-Ti oxide ore layers may occur in

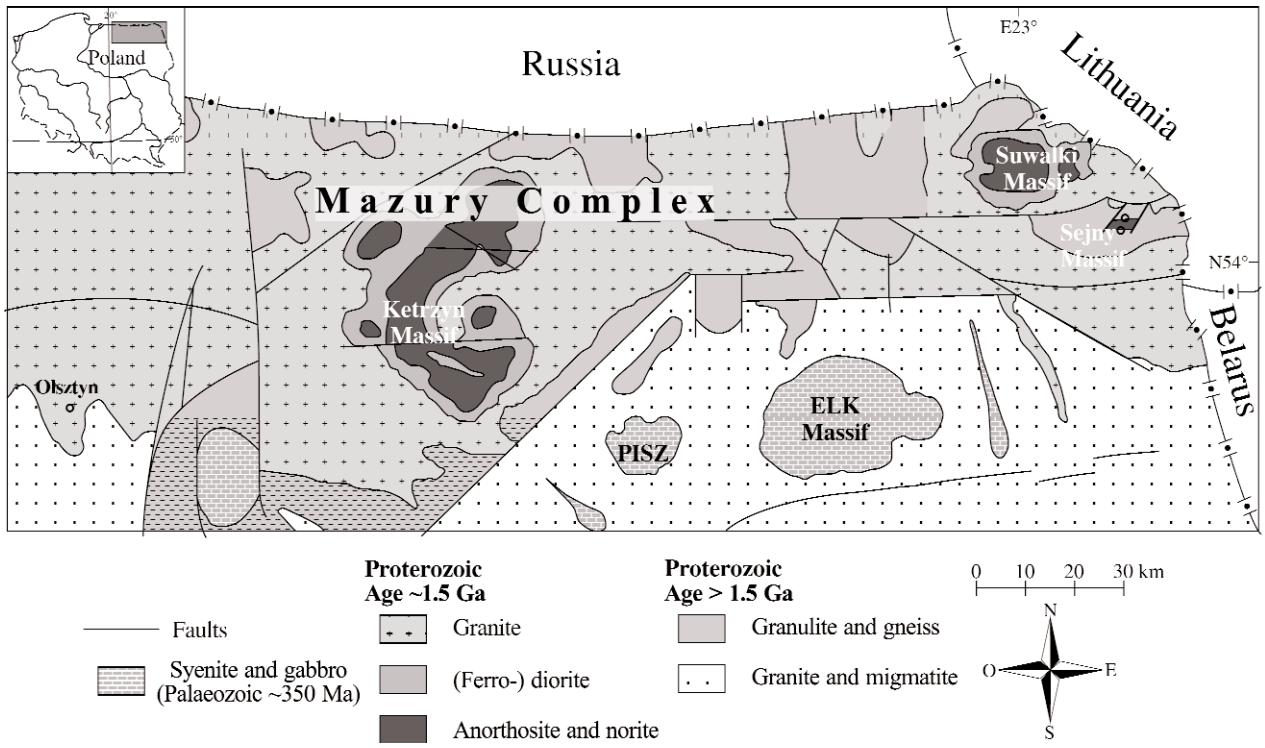

FIG. 1. Geologic map of the Mazury Complex. The complex extends westward some 180 to 200 km to the Baltic sea, and eastward ca. 30 km in Lithuania and Belarus (after Wiszniewska et al., 2002).

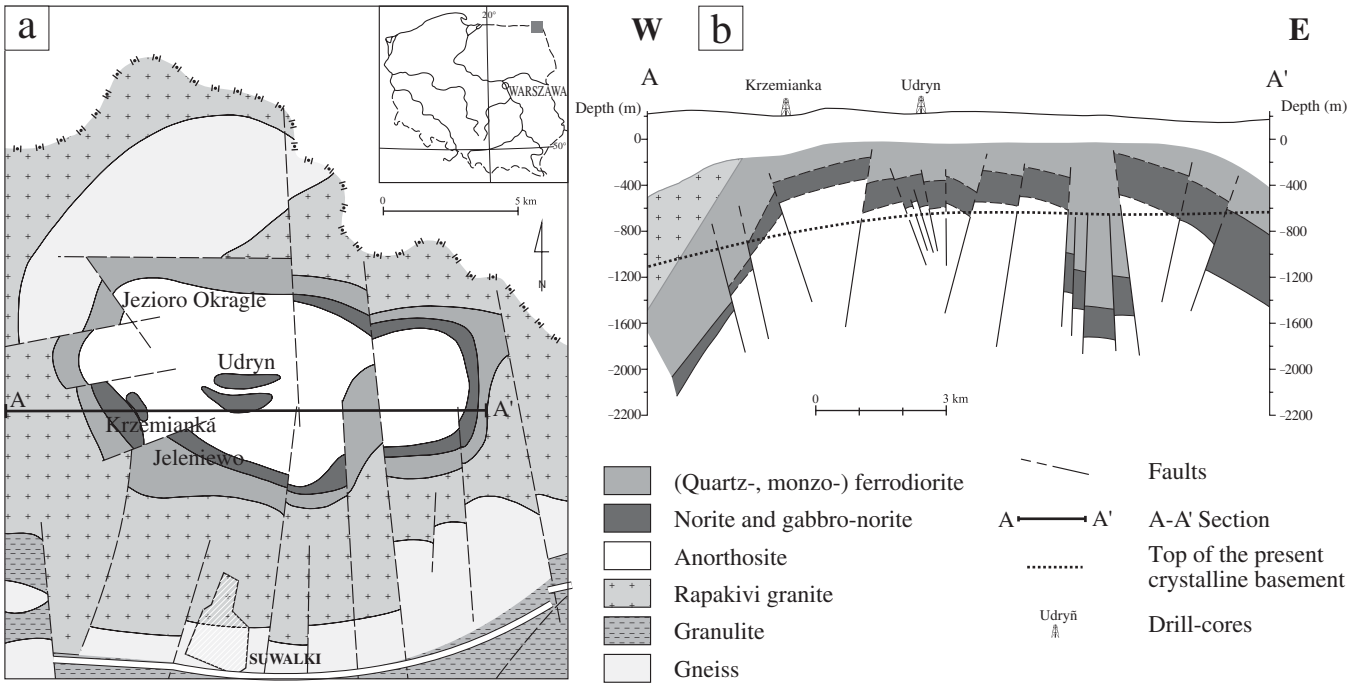

FIG. 2. a. Geologic map of the Suwalki anorthosite in northeastern Poland (with the location of Fe-Ti oxide ores); b. Cross section through the Suwalki anorthosite dome. Rock types and structures below the top of the present crystalline basement (dotted line dipping to the west) are interpreted from data on boreholes, while rocks and the initial crystalline basement above the dotted line are extrapolated (Juskowiak, 1998).

anorthosites, norites, and gabbronorites. They commonly dip southwest at an angle of 45° in Krzemianka and to the west at an angle of 45° in Udryn. Although the correlation between boreholes is difficult, a tentative reconstruction by Parecki (1998) of the distribution of Fe-Ti oxide ores in these two localities is presented in Figure 3. In a vertical section, the lower part is characterized by thick and wide oxide ores occurring in anorthosite. The correlation of orebodies between different boreholes in the upper part is much more complicated than in the lower part. Individual orebodies are up to 1,500 × 1,000 × 230 m thick.

Sampling and Analytical Methods

Twelve 10-cm-diameter boreholes drilled in the Suwalki anorthosite have been selected for this study. These boreholes, which reached 2,600 m depth, crosscut three ore

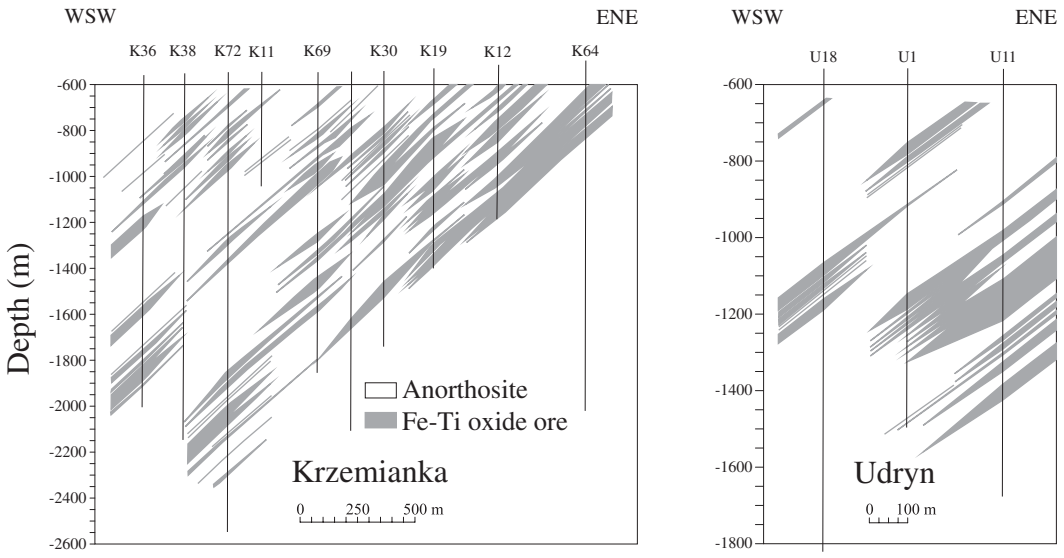

FIG. 3. Cross sections in the Krzemianka and Udryn deposits showing the distribution of Fe-Ti oxide ore lenses in the host anorthosite and related rocks (after Parecki, 1998).

deposits: Krzemianka, Udryn, and Jeleniewo. A series of coarse-grained Fe-Ti oxide ores representative of a portion of ca. 50 cm of a split drill core have been collected. Modal proportions for 35 samples have been determined by counting 1,000 points per 3 × 4.5 cm thin section.

Some samples have been selected for mineral separation of plagioclase and magnetite. The separation of the 60- to 150-µm fraction was performed with heavy liquids (bromoform and Clerici's solution) and a Frantz isodynamic magnetic separator. Plagioclase was analyzed for major elements (Si, Ti, Al, Fe, Ca, Na, K) by XRF, using an ARL 9400 XP at the University of Liege, on lithium-borate fused glass and for trace elements (Sr and Ba) on pressed powder pellets. Magnetite was analyzed for major elements (Si, Ti, Al, Fe, Mn, Mg) and for trace elements (Ni, V, Cr, Zn) by XRF following the method of Duchesne and Bologne (2009). The composition of orthopyroxene, ilmenite, clinopyroxene, olivine, and spinel was determined in selected samples by microprobe analysis with a Cameca SX50 at Bochum University. Standard operating conditions were excitation voltage of 15 kV and beam current of 15 nA. The following standards were used: pyrope for Mg and Al, andradite for Si, Fe, and Ca, spessartine for Al and Mn, rutile for Ti, jadeite for Na, ZnO for Zn, Cr_2O_3 for Cr, and metal V for V. Seventeen coarse-grained samples were analyzed for major and some trace elements by XRF following the method of Bologne and Duchesne (1991).

Petrography

Paragenesis, modal proportions, and spatial variations

The Suwalki anorthosite is massive and heterogranular (0.5 mm to >5 cm). It is essentially composed of antiperthitic plagioclase and may contain minor amounts of orthopyroxene, Ti magnetite, and ilmenite. The anorthosite usually displays gradual contacts with norites and Fe-Ti oxide ores, with continuous variations of modal proportions. Rocks may be massive but are commonly layered, locally with abrupt changes from oxide rich to anorthosite layers (Fig. 4).

Fe-Ti oxide ores display large variations in modal proportions (Table 1). Plagioclase, usually bent or recrystallized (ca. 1 cm), magnetite and ilmenite are the dominant phases. The primary texture of rocks has been modified by textural equilibration, which is a common feature in anorthositic rocks (Lafrance et al., 1996). Fe-Ti oxides have an interstitial habit as a result of subsolidus grain boundary readjustment (Duchesne, 1996). Orthopyroxene contains numerous Schiller lamellae of Fe-Ti oxides (Fig. 5a) and is sub- to euhedral. Its proportion ranges from 0 to 25 vol percent. Plagioclase lamellae in orthopyroxene from Fe-Ti ores have not been observed although they have been described in orthopyroxene megacrysts by Wiszniewska et al. (2002). In a few samples, an olivine corona is developed around orthopyroxene (Fig. 5b), either in contact with Fe-Ti oxides or plagioclase. Clinopyroxene commonly occurs as exsolutions in orthopyroxene and

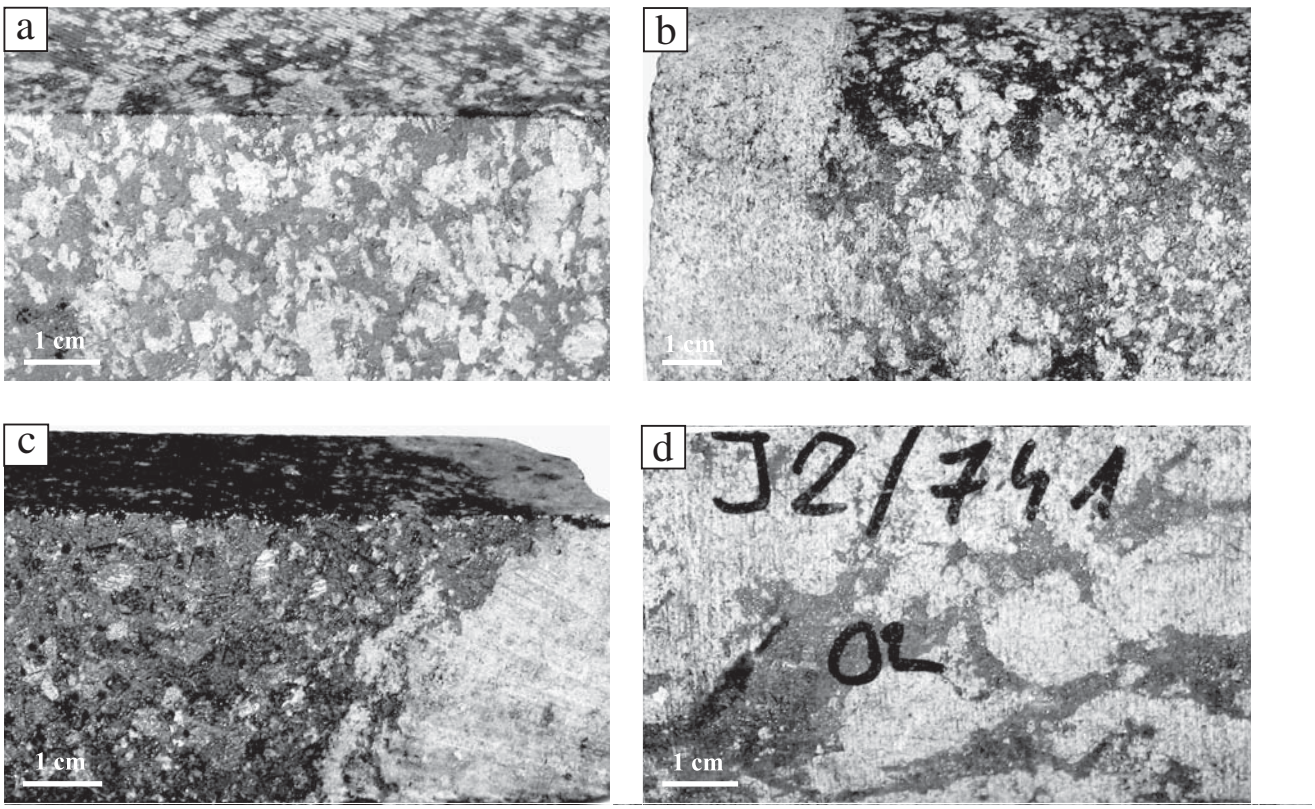

FIG. 4. Photographs of the main macroscopic textures of Fe-Ti oxide ores in the Suwalki anorthosite. a. Melanoritic ore with oriented plagioclase laths (K20-04); b. Layered ore with sharp contact between anorthosite and melanorite (U5-03); c. Massive ore with abrupt change from pure oxide to anorthosite layers (U4-04); d. Disseminated ore with interstitial character of Fe-Ti oxides (J2-02).

TABLE 1. Modal Proportions (vol %) of Selected Fe-Ti Oxide Ores from the Suwalki Anorthosite

	Depth (m)		Plag	Mag	Ilm	Opx	Cpx	Apatite	Olivine	Phlogopite	Al-Spinel	Sulfides
K2-01	1014	pmih-C	30.9	39.1	15.6	4.6				3.1	2.1	4.6
K2-02	1082	pmih-C	36.0	28.6	17.0	5.6				4.2	6.2	2.4
K2-05	1123	pmi-C	16.1	51.4	24.3	1.4				1.0	5.4	0.4
K12-02	989	pmih-C	47.8	25.6	6.2	15.8				1.0	2.0	1.6
K12-04	1060	pmih-C	24.9	36.5	10.8	20.2				3.4	1.5	2.7
K12-05	1453	pmihc-C	57.0	11.8	6.2	13.6	8.2			2.8		0.4
K20-03	1611	pmi-C	25.8	54.0	8.1	1.9			2.6	2.1	3.6	1.9
K20-04	1622	pmi-C	29.8	54.2	7.2	1.8			1.2	1.4	1.8	2.6
K20-05	1721	pmih-C	25.3	48.2	5.5	11.1			1.8	1.6	5.9	0.6
K20-06	1735	pmi-C	3.5	64.8	12.4	1.1			1.8	0.2	14.5	1.7
K20-07	1813	pmih-C	33.4	43.4	6.0	9.4			2.9	0.6	2.8	1.5
K20-08	1863	pmi-C	0.5	67.7	23.0	0.0			0.2	0.1	7.4	1.1
K20-09	1903	pmih-C	7.6	46.0	20.4	12.4				1.6	10.8	1.2
K22-01	1717	pmih-C	32.3	40.5	15.4	4.0			2.6	0.9	3.8	0.5
K48-03	1122	pmi-C	0.0	66.2	23.9	0.6				0.2	9.0	0.1
K57-02	337	pmih-C	27.0	36.2	20.0	9.2				1.2	6.2	0.2
K73-01	1851	pmih-C	24.7	39.9	21.8	6.7				1.2	4.2	1.5
U2-01	1144	pmih-C	41.4	18.8	10.9	24.9				2.5		1.5
U2-02	1169	pmih-C	31.2	28.0	15.5	18.5				2.6	0.3	3.9
U2-03	1339	pmihca-C	53.4	6.5	8.1	12.2	14.3	3.1		1.6		0.8
U2-04	1397	pmihca-C	35.1	9.3	8.1	22.1	17.8	4.0		2.4		1.2
U2-06	1512	pmih-C	11.0	52.1	21.5	9.2				2.2	3.4	0.6
U4-01	1168	pmih-C	56.8	15.2	11.6	13.1				1.8		1.5
U4-02	1205	pmihca-C	42.9	7.4	9.7	14.6	18.5	5.2		1.3		0.4
U4-03	1257	pmih-C	21.4	50.0	7.1	10.2			2.1	4.4	1.7	3.1
U4-04	1330	pmih-C	8.7	57.4	18.9	7.1				1.4	6.2	0.3
U4-05	1379	pmih-C	11.9	54.0	20.2	4.8				2.8	5.4	0.9
U4-06	1408	pmi-C	1.0	65.0	23.6	0.8				0.4	9.0	0.2
U5-02	1256	pmih-C	52.6	15.8	7.6	19.2				1.4	0.4	3.0
U5-04	1373	pmi-C	3.6	70.8	14.5	1.8			0.3		8.7	0.3
J1-01	1124	pmih-C	26.9	46.4	14.2	5.6				2.2	0.3	4.4
J1-02	1240	pmihca-C	50.4	9.3	7.8	18.9	8.2	2.8		1.3	0.2	1.1
J2-01	1305	pmih-C	49.4	22.9	14.8	8.7				2.6	0.4	1.2
J2-02	1561	pmih-C	44.7	33.8	10.9	3.0				3.2	3.8	0.6
J2-03	1584	pmih-C	42.6	33.0	8.4	7.5				3.3	4.2	1.0

Drill core labels: K = Krzemianka, U = Udryn, J = Jeleniewo; K12 = core number; -02 = sample number

Drill core locations: (54°N-22°E): K2 (12'11"N-51'46"E) - K12 (12'47"N-52'53"E) - K20 (13'01"N-52'33"E) - K22 (13'17"N-52'44"E) - K48 (13'74"N-51'40"E) - K57 (13'31"N-52'47"E) - K73 (12'25"N-51'91"E) - U2 (13'28"N-57'07"E) - U4 (13'21"N, 57'03"E) - U5 (13'30"N, 56'39"E) - J1 (11'49"N, 54'40"E) - J2 (11'45"N, 54'55"E)

Samples with <2 vol % of orthopyroxene are referred to as pmi-C

a few samples also contain prismatic grains (8–18 vol %; Fig. 5c). Most samples with clinopyroxene also contain apatite (3–5 vol %). Aluminous spinel (Fig. 5d) is always in contact with magnetite and ilmenite. Its proportion (0–15 vol %) is directly correlated with the amount of Fe-Ti oxides. Ti-rich phlogopite (Namur et al., 2009) and Ni-Cu sulfides are common.

We use the nomenclature of Irvine (1982) for Fe-Ti oxide-enriched rocks, which are named according to the first letter of the main phases followed by -C meaning "cumulus". This nomenclature gives a clear picture of the parageneses of the rocks but should not be considered a genetic classification. The most common assemblages in Suwalki Fe-Ti ores are as follows: plagioclase (p) + magnetite (m) + ilmenite (i) (pmi-C) and plagioclase (p) + magnetite (m) + ilmenite (i) + orthopyroxene (h) (pmih-C). The limit between these two types of rocks has been fixed at 2 vol percent of orthopyroxene. Some rocks also contain clinopyroxene (c) (pmihc-C), most often with apatite (a) (pmihca-C).

On a large scale, the lower parts of Krzemianka and Udryn deposits are made up of oxide ores in anorthosite (pmi-C and pmih-C with low proportions of orthopyroxene), whereas the upper is dominated by noritic ores (pmih-C and pmihca-C with higher proportions of orthopyroxene). The contact between oxide ores and anorthosite may be sharp or gradual, producing rocks ranging from pure anorthosite to massive oxide ore. In any case, anorthosite-ore contacts in the lower part of the orebodies are sharper compared to the upper part displaying gradational anorthosite/ore transitions.

Subsolidus reequilibration of Fe-Ti oxides

Fe-Ti oxides display numerous microtextures resulting from subsolidus re-equilibration (e.g., Duchesne, 1972). Magnetite exhibits cloth and trellis microtextures (Fig. 6a, b) which occur primarily as very fine ulvöspinel (Fe_2TiO_4) lamellae which have been completely oxidized to ilmenite. The oxidation of magnetite to form a trellis microtexture can also produce external granules of ilmenite. Aluminous spinel lenses are also exsolved from magnetite and more locally from ilmenite and may form external granules (Fig. 6b). Ilmenite grains commonly lack hematite lamellae but locally contain some aluminous spinel blebs (Fig. 6c). Compositional reequilibration between magnetite and ilmenite produces a variety

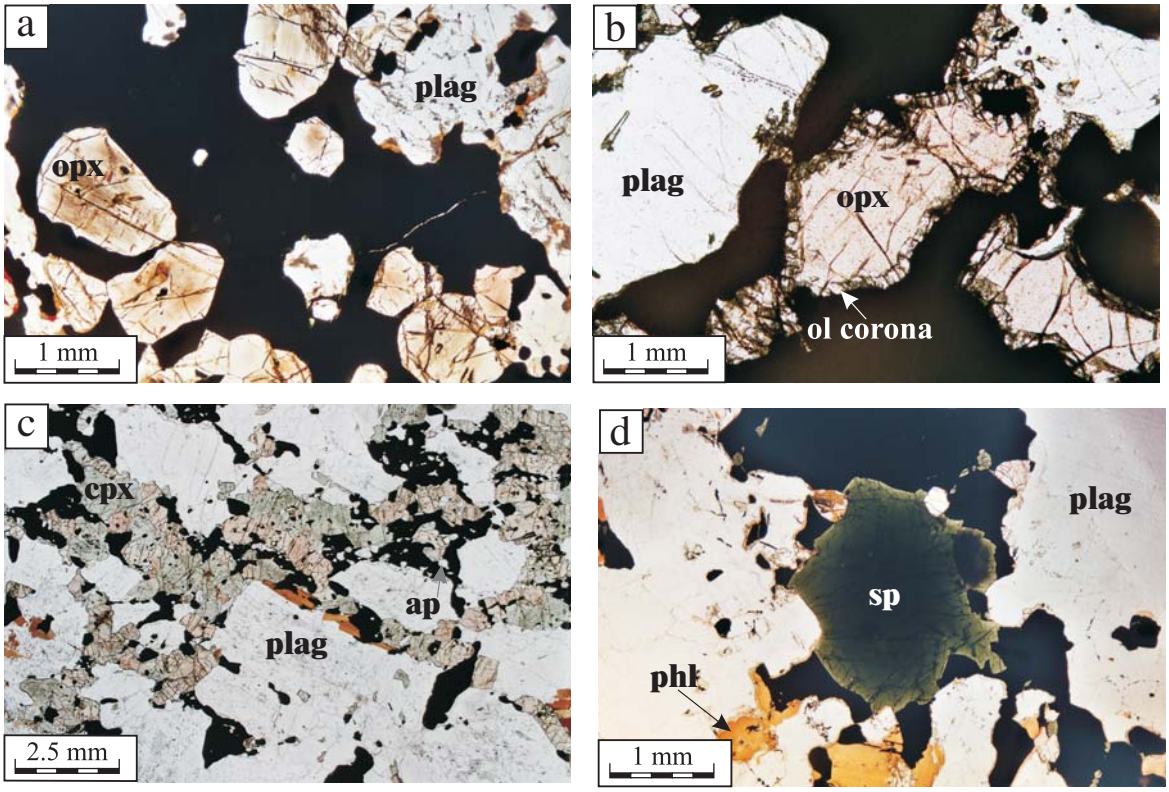

FIG. 5. Photomicrographs of the main textures observed in Fe-Ti oxide ores of the Suwalki anorthosites (transmitted light). a. pmih-C with euhedral orthopyroxene containing Schiller lamellae (K12-02); b. pmih-C with olivine coronas around orthopyroxene (K22-01); c. pmihac-C displaying oriented plagioclase laths (U2-03). d. Large zoned aluminous spinel grain (J2-03); Mineral abbreviations: plag = plagioclase, opx = orthopyroxene, ilm = ilmenite, mt = magnetite, ap = apatite, ol = olivine, sp = aluminous spinel, phl = phlogopite.

of contact textures with aluminous spinel-bearing ilmenite rims (Fig. 6d). Because of these subsolidus processes, the bulk composition of reequilibrated magnetite cannot be determined by in situ methods. Therefore, the composition of magnetite has been determined through bulk analyses of mineral separates. Nevertheless, external granules of ilmenite and aluminous spinel might also have been removed during the magnetic separation process and, therefore, our analyses might be slightly different from the liquidus compositions.

Analytical Data

The composition of Fe-Ti oxides and aluminous spinel

The TiO_2 content of magnetite ranges from 0 to 7.77 wt percent (Table 2), corresponding to a calculated proportion of ulvöspinel (Usp) from 0 to 23.6 mol %. Al_2O_3 (0.46–4.44 wt %), MnO (0.02–0.28 wt %), and MgO (0.12–1.40) in magnetite are positively correlated with the Usp content. Chromium is a highly compatible element in magnetite and may be considered a differentiation index. Cr in magnetite usually decreases upwards in each drill-core and is the lowest in pmihca-C and the highest in Fe-Ti oxide-rich rocks (Fig. 7a).

Ilmenite has a hematite content from 1.2 to 8.6 mol percent (Table 3)—thus, usually it is below the threshold of exsolution. Hematite exsolution is therefore only observed in small amounts in a few samples (e.g., U2-04). The hematite content of ilmenite is highly correlated with the magnetite/ilmenite ratio (Fig. 7b). The MgO content (0.55–3.56 wt %), very sensitive to subsolidus reequilibration (Charlier et al., 2007), is negatively correlated with the MnO content (0.68–1.19 wt %). The composition of both magnetite and ilmenite cannot be used to discriminate the different occurrences.

The molar Mg/Fe ratio of aluminous spinel is close to 1 (Table 4), which is actually the limit between hercynite and spinel. No significant compositional variations have been observed between aluminous spinel occurring either as large external granule exsolutions (Figs. 5a, 6b), as discrete lamellae in magnetite and ilmenite (Fig. 6a), or as small grains in the reaction rim between ilmenite and magnetite (Fig. 6d). From sample to sample, $X_{hercynite}$ varies from 0.405 to 0.636 (Table 4). The ZnO and MnO contents are low, reflected by low fractions of $X_{gahnite}$ (0.008–0.076) and $X_{galaxite}$ (0.003-0.005). As illustrated in Fig. 5a, large grains of aluminous spinel are zoned with a higher $X_{hercynite}$ content in the core and a continuous X_{spinel} enrichment towards the margin. Note that when in contact with a silicate phase (with, e.g., plagioclase in Fig. 5a), aluminous spinel is not zoned. This suggests that the zoning (Fe-rich core and Mg-rich rim) results from postexsolution reequilibration with Fe-Ti oxides.

The composition of silicate minerals

Plagioclase composition ranges from labradorite to andesine with an anorthite content from $An_{60.0}$ to $An_{43.6}$ and an orthoclase content from $Or_{0.2}$ to $Or_{4.3}$ (Table 5). There is a broad

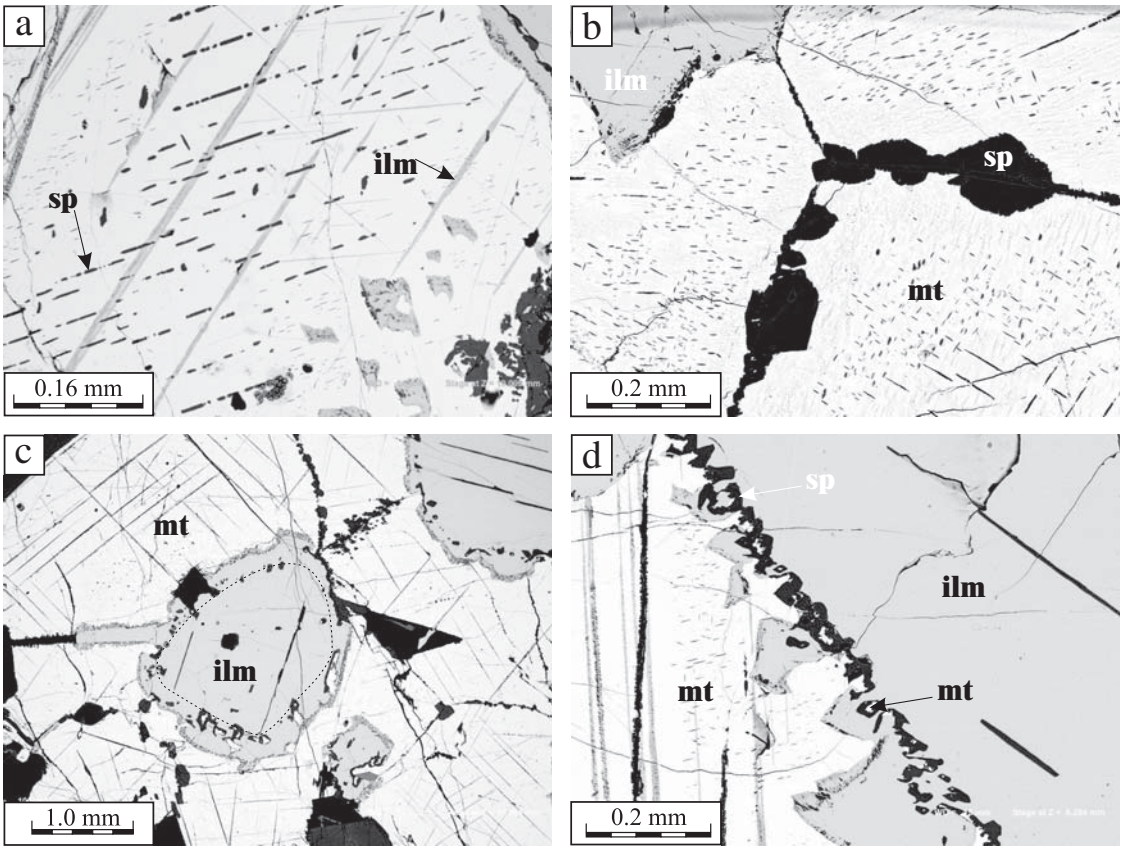

FIG. 6. Backscattered electron images of exsolution types in magnetite and reequilibration textures between magnetite and ilmenite. a. Trellis-textured magnetite grain with ilmenite and aluminous spinel exsolutions (K20-05); b. Cloth-textured magnetite with oxidized ulvöspinel and aluminous spinel lamellae in (100) planes. Note the zone without aluminous spinel along the grain boundaries and the external granules of aluminous spinel (K20-03). c. Ilmenite grain surrounded by magnetite. The hypothetical primary contour of ilmenite (indicated by the dotted line) is marked by aluminous spinel crystals, which locally contain relict of magnetite (K2-05); d. Irregular contact between ilmenite and magnetite with a discontinuous rim of aluminous spinel-rich ilmenite. Note the relicts of magnetite observed in some of the aluminous spinel grains (K20-05).

TABLE 2. Magnetite Composition (XRF analyses on mineral separates) from Fe-Ti Ores of the Suwalki Anorthosite

	Depth (m)		SiO_2	TiO_2	Al_2O_3	Fe_2O_3	FeO	MnO	MgO	Total	Usp	Ni	V	Cr	Zn
K12-02	989	pmih-C	0.38	2.25	2.90	61.69	32.78	0.10	0.54	100.64	6.6	785	4317	562	843
K12-04	1060	pmih-C	0.61	6.26	4.04	52.43	35.64	0.24	1.02	100.24	18.9	657	4018	455	829
K12-05	1453	pmihc-C	0.48	3.46	2.79	58.89	33.38	0.11	0.67	99.78	10.3	290	4737	397	1182
K20-03	1611	pmi-C	0.33	7.77	3.97	49.37	37.00	0.27	0.96	99.67	23.6	564	3773	501	811
K20-05	1721	pmih-C	0.28	6.19	4.28	52.48	35.39	0.19	1.23	100.04	18.8	745	5068	1377	458
K20-06	1735	pmi-C	0.05	5.89	3.99	53.39	34.74	0.19	1.40	99.65	17.8	763	5712	1399	273
K20-09	1903	pmih-C	0.07	0.87	1.95	65.13	31.45	0.03	0.42	99.92	2.5	644	6739	2861	73
K22-01	1717	pmih-C	0.45	6.66	4.44	51.17	35.87	0.21	1.14	99.94	20.3	628	4923	1157	537
K48-03	1122	pmi-C	0.00	5.49	3.08	54.61	34.77	0.22	0.90	99.07	16.4	620	5384	2719	382
K73-01	1851	pmih-C	0.03	1.00	1.87	64.82	31.18	0.06	0.59	99.55	2.9	421	5918	2800	281
U2-01	1144	pmih-C	0.26	2.81	2.38	60.85	33.12	0.10	0.50	100.02	8.3	250	5055	725	1117
U2-04	1397	pmihca-C	0.21	1.08	1.28	65.50	31.67	0.07	0.32	100.13	3.1	183	2520	210	1863
U2-06	1512	pmih-C	0.23	5.24	4.03	53.93	34.95	0.12	0.81	99.31	16.1	791	4951	5330	617
U4-01	1168	pmih-C	0.28	2.95	2.46	60.57	33.33	0.13	0.46	100.18	8.6	530	4801	1002	1638
U4-03	1257	pmih-C	0.33	7.41	3.66	50.24	36.54	0.28	0.95	99.41	22.4	787	4196	1615	817
U4-05	1379	pmih-C	0.00	4.73	3.53	55.23	34.70	0.14	0.56	98.89	14.4	694	4890	6781	488
U5-01	1035	pmihca-C	0.43	0.00	0.46	68.85	31.05	0.02	0.12	100.93	0.0	35	2012	170	266
U5-02	1256	pmih-C	0.18	3.09	2.53	60.13	33.18	0.10	0.62	99.83	9.2	358	4992	628	1630
U5-04	1373	pmi-C	0.23	4.44	3.54	55.89	34.13	0.13	0.77	99.13	13.5	839	5025	4371	377
J1-01	1124	pmih-C	0.19	4.28	3.02	57.28	33.96	0.17	0.82	99.72	12.7	620	4926	969	751
J2-01	1305	pmih-C	0.58	0.64	1.75	65.19	30.85	0.05	0.46	99.52	1.8	163	5212	1068	1088

Major elements in wt percent, FeO and Fe_2O_3 recalculated from Fe_2O_{3tot} by charge balance; molar fractions of ulvöspinel (Usp) calculated following QUILF algorithm (Andersen et al. 1993); trace elements in parts per million (ppm)

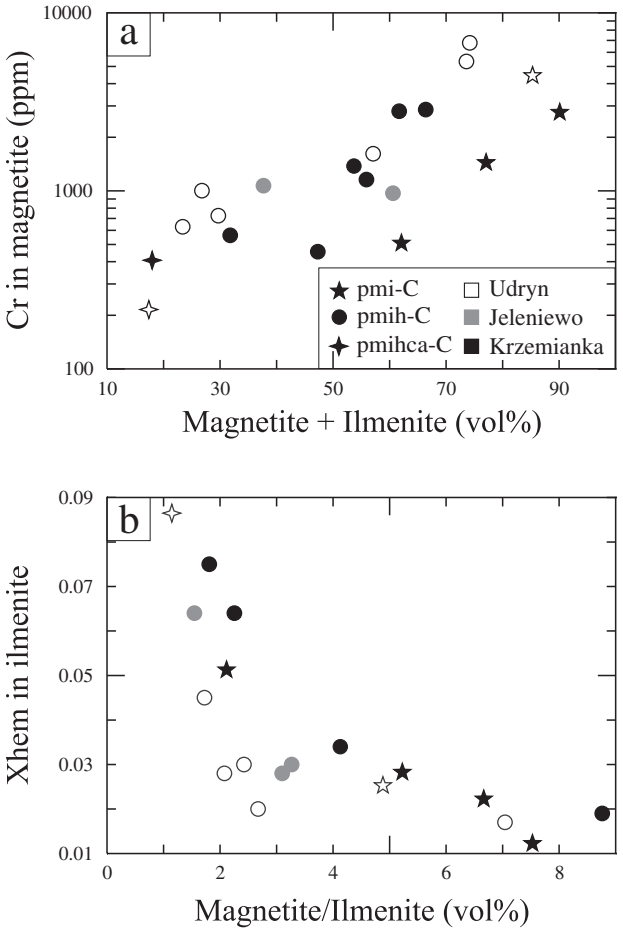

FIG. 7. Composition of magnetite and ilmenite as a function of their modal proportions. a. Cr content of magnetite (ppm) vs. modal proportions (vol %) of magnetite + ilmenite. b. Molar fraction of hematite in ilmenite vs. the ratio of the modal proportions (vol %) of magnetite/ilmenite. Different symbols are used to discriminate the minerals assemblages while different grays are used for the occurrences.

correlation between the An content of plagioclase and the Cr content in magnetite (Fig. 8a). Plagioclase from Krzemianka ores is poorer in Sr and Ba compared to plagioclase from Udryn (Fig. 8b).

The composition of orthopyroxene ranges from $En_{76.6}$ to $En_{59.9}$ (Table 6). The Mg# decreases upward in each drill core and is negatively correlated with the proportion of Fe-Ti oxides (Fig. 8c). MnO (0.26–1.26 wt %) increases with decreasing Mg# reflecting the increase with fractionation. The Al_2O_3 content of orthopyroxene spans a wide range from 1.06 to 4.95 wt % and is positively correlated with the Mg# (Fig. 8d). As previously described, orthopyroxene is locally surrounded by an olivine corona (Fig. 5c, d). The composition of olivine in four of these samples ranges from $Fo_{75.3}$ to $Fo_{64.4}$ (Table 6), whereas the associated orthopyroxene composition ranges from $En_{69.9}$ to $En_{76.6}$. The Mg# of clinopyroxene ranges from 70.4 to 68.5 (Table 6).

Whole-rock composition

Seventeen whole-rock analyses (Table 7) are plotted in major element binary diagrams (Fig. 9). SiO_2 has been chosen as the variation index, as it is essentially correlated with the modal abundance of plagioclase and orthopyroxene in the cumulates. Compositional ranges of main phases (plagioclase, orthopyroxene, magnetite, ilmenite, clinopyroxene, and aluminous spinel) are also plotted.

Whole-rock compositions display a large range: SiO_2 0.46–41.58 wt percent; TiO_2 4.36–12.96 wt percent; Fe_2O_{3tot} 22.98–76.25 wt percent. Rocks with plagioclase, magnetite, and ilmenite (pmi-C) are the most melanocratic (Fe_2O_{3tot} and TiO_2 richest), although there are continuous trends with orthopyroxene-bearing rocks (pmih-C). This is concordant with the continuous range of orthopyroxene proportion from 0 to 25 vol percent (Table 1). Clinopyroxene and apatite-bearing rocks are the most leucocratic (SiO_2-richest) and have a significantly higher CaO content. V, Cr, and Zn are positively correlated with Fe_2O_{3tot} and TiO_2 (not shown) and thus with

TABLE 3. Microprobe Analyses of Ilmenite from Fe-Ti Ores of the Suwalki Anorthosite

	Depth (m)	n		TiO_2	Al_2O_3	Fe_2O_3	FeO	MnO	MgO	Total	Xgeik	Xpyr	Xhem	Xilm
K2-05	1123	3	pmi-C	50.51	0.05	5.41	41.83	0.92	1.49	100.21	0.055	0.019	0.051	0.874
K12-02	989	6	pmih-C	51.18	0.06	3.64	42.52	0.91	1.45	99.76	0.054	0.019	0.034	0.892
K20-03	1611	5	pmi-C	52.44	0.05	2.41	42.41	0.74	2.24	100.29	0.083	0.016	0.022	0.879
K20-04	1622	7	pmi-C	52.88	0.06	1.30	41.30	0.68	3.12	99.34	0.115	0.014	0.012	0.858
K20-05	1721	6	pmih-C	52.33	0.05	1.99	42.41	0.72	2.20	99.70	0.082	0.015	0.019	0.884
K20-06	1735	14	pmi-C	52.81	0.11	3.04	40.44	0.69	3.56	100.65	0.130	0.014	0.028	0.828
K20-09	1903	19	pmih-C	49.91	0.05	6.78	41.52	0.73	1.47	100.46	0.055	0.015	0.064	0.866
K57-02	337	7	pmih-C	48.99	0.05	7.93	39.81	0.79	1.93	99.50	0.072	0.017	0.075	0.836
U2-01	1144	5	pmih-C	50.52	0.06	4.74	41.75	0.82	1.60	99.49	0.060	0.017	0.045	0.878
U2-04	1397	10	pmihca-C	48.73	0.07	9.12	40.01	1.19	1.46	100.58	0.054	0.025	0.086	0.835
U2-06	1512	14	pmih-C	51.86	0.03	3.25	43.63	0.78	1.24	100.80	0.046	0.016	0.030	0.907
U4-03	1257	5	pmih-C	52.58	0.05	1.83	42.28	0.78	2.36	99.88	0.087	0.016	0.017	0.879
U4-05	1379	4	pmih-C	51.65	0.04	2.12	44.27	0.85	0.74	99.67	0.028	0.018	0.020	0.934
U5-02	1256	5	pmih-C	51.58	0.06	3.03	42.03	0.85	1.96	99.51	0.073	0.018	0.028	0.880
U5-04	1373	8	pmi-C	51.33	0.05	2.58	43.13	0.89	1.19	99.17	0.045	0.019	0.025	0.912
J1-01	1124	14	pmih-C	51.98	0.04	3.24	42.64	1.04	1.71	100.66	0.063	0.022	0.030	0.885
J2-01	1305	16	pmih-C	49.60	0.04	6.84	42.54	1.07	0.55	100.64	0.021	0.023	0.064	0.892
J2-02	1561	2	pmih-C	51.50	0.05	2.99	41.86	0.80	2.04	99.24	0.076	0.017	0.028	0.879

Major elements in wt percent, FeO and Fe_2O_3 recalculated from Fe_2O_{3tot} by charge balance; molar fractions of geikielite, pyrophanite, hematite, and ilmenite (Xgeik, Xpyr, Xhem, Xilm) calculated following QUILF algorithm (Andersen et al., 1993); n = number of microprobe analyses

TABLE 4. Microprobe Analyses of Aluminous Spinel from Fe-Ti Ores of the Suwalki Anorthosite

	Depth (m)	n		TiO_2	Al_2O_3	FeO	MgO	MnO	Cr_2O_3	ZnO	V_2O_3	Total	Xherc	Xspinel	Xgal	Xgah
K2-01	1014	12	pmih-C	0.02	60.90	23.36	12.08	0.19	0.14	1.83	-	98.52	0.500	0.461	0.004	0.035
K2-02	1082	8	pmih-C	0.12	59.80	25.64	11.60	0.19	0.43	0.84	-	98.62	0.543	0.438	0.004	0.016
K2-05	1123	10	pmi-C	0.27	61.45	23.40	12.87	0.19	0.50	1.06	-	99.74	0.493	0.483	0.004	0.020
K12-02	989	3	pmih-C	0.03	59.90	26.79	9.90	0.25	0.14	2.17	0.06	99.24	0.575	0.379	0.005	0.041
K20-04	1622	8	pmi-C	0.05	60.78	23.37	12.93	0.18	0.14	1.42	-	98.87	0.488	0.482	0.004	0.026
K20-06	1735	3	pmi-C	0.38	62.36	19.99	16.11	0.13	0.34	0.61	0.07	99.99	0.405	0.582	0.003	0.011
K20-09	1903	4	pmih-C	0.23	61.76	24.01	12.54	0.19	0.65	0.42	0.09	99.89	0.512	0.476	0.004	0.008
K22-01	1717	8	pmih-C	0.07	60.58	24.84	12.18	0.16	0.26	1.03	-	99.12	0.522	0.456	0.003	0.019
U2-06	1512	7	pmih-C	0.36	58.85	27.99	10.26	0.19	1.05	1.17	0.07	99.94	0.589	0.385	0.004	0.022
U4-05	1379	2	pmih-C	0.42	58.40	29.25	8.75	0.21	1.42	1.03	0.05	99.53	0.636	0.339	0.005	0.020
U5-04	1373	2	pmi-C	0.04	58.66	27.83	10.59	0.20	0.72	1.01	0.09	99.14	0.582	0.395	0.004	0.019
J1-01	1124	2	pmih-C	0.55	61.55	22.74	12.32	0.20	0.25	2.34	0.03	99.98	0.484	0.468	0.004	0.044
J2-01	1305	3	pmih-C	0.68	62.00	21.03	11.86	0.21	0.27	3.94	0.07	100.06	0.459	0.461	0.005	0.076
J2-02	1561	8	pmih-C	0.06	59.40	25.69	11.53	0.18	0.44	1.18	-	98.48	0.541	0.433	0.004	0.022
J2-03	1584	8	pmih-C	0.09	60.10	24.72	12.76	0.17	0.74	0.78	-	99.36	0.512	0.471	0.004	0.014

Xherc, Xspinel, Xgal and Xgah are molar fractions of hercynite ($FeAl_2O_4$), spinel ($MgAl_2O_4$), galaxite ($MnAl_2O_4$) and gahnite ($ZnAl_2O_4$) respectively; n is the number of microprobe analyses

TABLE 5. Plagioclase Composition (XRF analyses on mineral separates) from Fe-Ti Ores of the Suwalki Anorthosite

	Depth (m)		SiO_2	TiO_2	Al_2O_3	Fe_2O_{3tot}	CaO	Na_2O	K_2O	Total	Sr	Ba	An[1]	O[2]
K12-02	989	pmih-C	55.30	0.04	28.92	0.14	9.88	4.87	0.20	99.35	893	286	52.9	1.3
K12-04	1060	pmih-C	55.46	0.05	28.73	0.22	9.77	5.32	0.11	99.66	927	256	50.4	0.7
K12-05	1453	pmihc-C	55.49	0.04	28.36	0.12	9.43	5.42	0.18	99.04	946	216	49.0	1.1
K20-03	1611	pmi-C	55.73	0.06	28.57	0.19	9.60	5.43	0.13	99.71	994	280	49.4	0.8
K20-05	1721	pmih-C	55.03	0.06	29.05	0.19	10.15	5.07	0.20	99.75	962	198	52.5	1.2
K20-06	1735	pmi-C	54.95	0.07	29.14	0.12	10.02	5.21	0.04	99.55	1025	150	51.5	0.2
K22-01	1717	pmih-C	55.03	0.06	28.93	0.25	10.02	5.03	0.29	99.61	918	206	52.4	1.8
K73-01	1851	pmih-C	54.89	0.07	29.11	0.60	9.58	5.07	0.07	99.39	928	199	51.1	0.4
U2-01	1144	pmih-C	55.29	0.04	28.18	0.25	9.50	5.16	0.51	98.93	918	529	50.4	3.1
U2-04	1397	pmihca-C	57.00	0.03	27.01	0.19	8.56	5.42	0.69	98.90	961	507	46.6	4.3
U2-06	1512	pmih-C	52.76	0.04	29.86	0.20	11.63	4.29	0.05	98.83	1117	177	60.0	0.3
U4-01	1168	pmih-C	55.98	0.04	28.29	0.22	9.49	5.24	0.34	99.60	956	353	50.0	2.1
U4-03	1257	pmih-C	55.36	0.07	28.23	0.20	9.26	5.43	0.13	98.68	1083	378	48.5	0.8
U5-01	1035	pmihca-C	59.73	0.03	25.80	0.25	7.68	5.50	0.13	99.12	1238	119	43.6	0.9
U5-02	1256	pmih-C	55.23	0.03	28.26	0.24	9.82	4.83	0.60	99.01	932	405	52.9	3.7
J1-01	1124	pmih-C	55.24	0.07	28.86	0.44	9.58	5.34	0.08	99.61	961	315	49.8	0.5
J2-01	1305	pmih-C	56.24	0.04	28.01	0.80	8.50	5.68	0.33	99.60	-	-	45.3	2.0

[1] An = 100 [Ca/(Ca+Na)]
[2] Or = 100 [K/(Ca+Na+K)]

the proportion of Fe-Ti oxides. In the Al_2O_3 versus SiO_2 diagram, the intercept at 0 wt percent SiO_2 above oxide compositions suggests the role of external granule exsolution of aluminous spinel for whole-rock compositions. It also shows that liquidus magnetite and ilmenite had initially higher Al_2O_3 contents before the exsolution process.

Liquidus Phases and Sequence of Crystallization

In Fe-Ti oxide-rich rocks, magnetite and ilmenite may be associated with plagioclase alone (pmi-C). This paragenesis essentially occurs in lower parts of the deposits, whereas the appearance of orthopyroxene (pmih-C) occurs at higher stratigraphic levels. At the highest stratigraphic levels and in the marginal zones, a few rocks also contain clinopyroxene ± apatite (pmihc-C and pmihca-C).

Although a sequence of crystallization cannot be clearly identified in the Suwalki anorthosite on the basis of stratigraphy, as it may be done in layered intrusions, the continuously increasing number of phases may be considered an index of differentiation. The sequence of crystallization in Fe-Ti oxide ores from the Suwalki anorthosite is thus plagioclase + magnetite + ilmenite, followed by orthopyroxene, clinopyroxene and finally by apatite. This sequence of crystallization is further supported by mineral compositions which show that pmihca-C are the most evolved rocks (lower Cr content of magnetite, lower Mg# of orthopyroxene). Moreover, even if Fe-Ti oxides display interstitial relationships relative to plagioclase and pyroxenes, which is a result of subsolidus grain boundary readjustment (Duchesne, 1996), they may be found included in these minerals, indicating that magnetite and ilmenite are early crystallizing minerals.

This order of liquidus phases appearance seems to be contradictory to the close relation between Fe-Ti oxide ores and the host anorthosite in which plagioclase + high-alumina orthopyroxene assemblages occur (Wiszniewska et al., 2002), which is an evidence that orthopyroxene may appear before

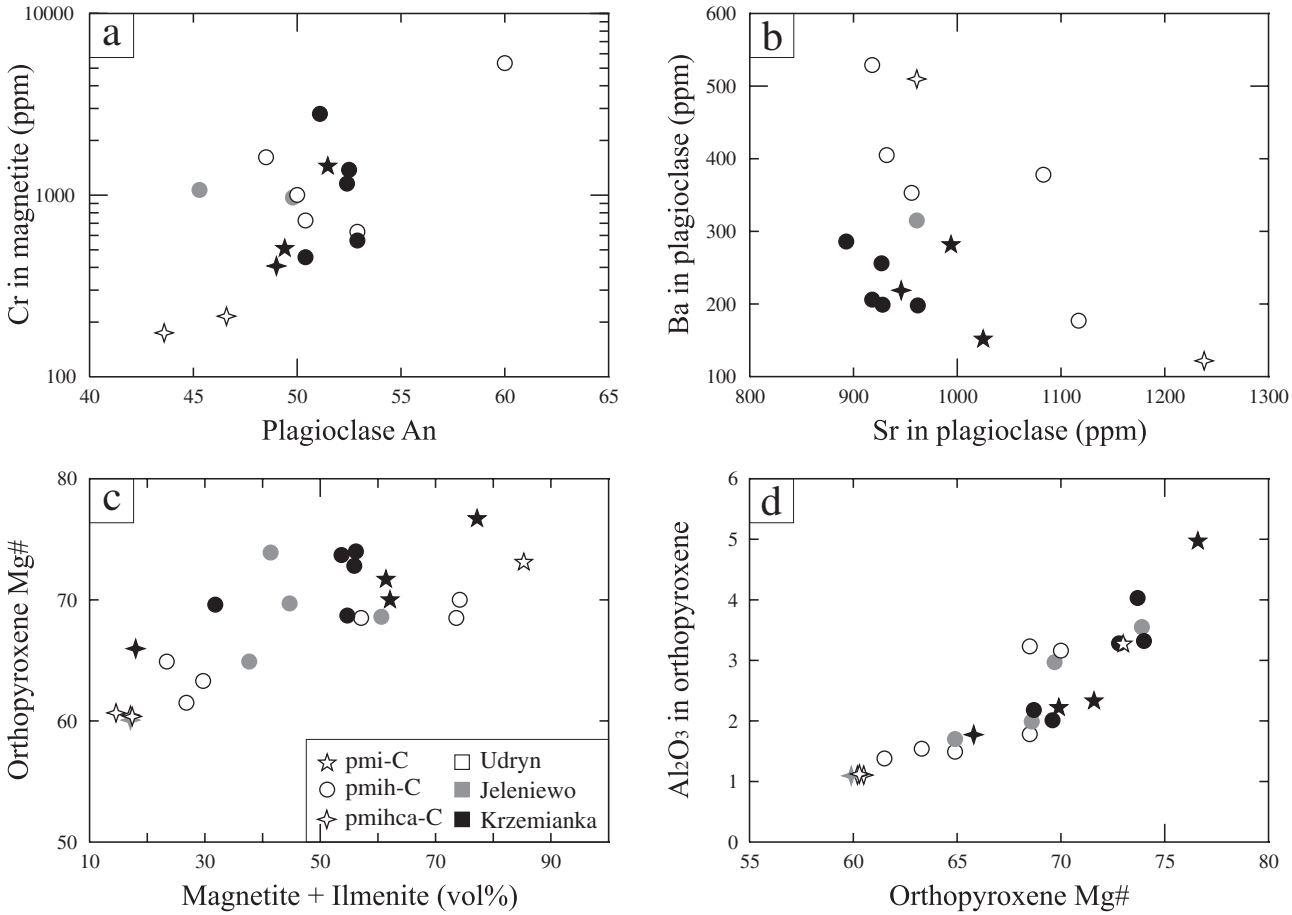

FIG. 8. Plots of mineral compositions and Fe-Ti oxides modal proportions. a. Cr content in magnetite vs. anorthite (molar %) in plagioclase. b. Ba vs. Sr contents of plagioclase (ppm). c. Mg# of orthopyroxene (molar %) vs. modal proportions (vol %) of magnetite + ilmenite. d. Al_2O_3 in orthopyroxene (wt %) vs. Mg# of orthopyroxene (molar %).

Fe-Ti oxides. However, as discussed later, both sequences of crystallization may result from a single parental magma if different pressures of crystallization are considered.

The Proportion of Liquidus Phases: Evidence for Crystal Sorting

Principal components analysis has been performed on whole-rock compositions in order to constrain the main controlling factors on compositional variations. The correlation matrix (Table 8) has been used to obtain factor loadings for whole-rock compositions (Table 9). Most of the variation in the data is explained by two principal components (Fig. 10), which together account for 88 percent of the variance. The first principal component represents 65 percent of the total variance and is heavily positively loaded by SiO_2, Al_2O_3, Na_2O, CaO, K_2O, and MgO and negatively by TiO_2 and Fe_2O_3. The variability of whole-rock compositions may thus be explained by the relative proportion of plagioclase and ferromagnesian silicates on one side and of Fe-Ti oxides on the other side. Principal component 2 (23% of the total variance) is essentially loaded by P_2O_5 and MnO. This component represents the compositional difference of more evolved cumulates with cumulus apatite, in which Fe-Ti oxides and pyroxenes are richer in MnO that behaves as an incompatible element.

The proportion of cumulus phases and thus the whole-rock compositions are controlled by the relative proportion of two poles: plagioclase and Fe-Mg silicates relative to Fe-Ti oxides. The good correlation between plagioclase and pyroxenes results from the high grade of pmi-C (low proportions of plagioclase and, by definition, less than 2 vol % of orthopyroxene) and the higher proportions of plagioclase and pyroxenes in pmih-C, pmihc-C, and pmihca-C. In Fe-Ti oxide ores from the Suwalki anorthosite, density contrast between liquidus phases ($\rho_{magnetite} = 5.2$; $\rho_{ilmenite} = 4.7$; $\rho_{opx\ (En65)} = 3.7$; $\rho_{cpx} = \sim 3.5$; $\rho_{apatite} = 3.3$; $\rho_{plagioclase\ (An50)} = 2.65$) thus plays an important role and is responsible for crystal sorting. However, the effectiveness of sorting decreases with the number of phases in the rocks, which results in lower Fe-Ti oxides in evolved rocks.

Oxygen Fugacity

Fe-Ti oxides thermo-oxybarometry and the QUILF equilibria

The cooling evolution and the reequilibration of the oxide mineral composition of the Suwalki deposit can be examined on the basis of (1) inter-oxide reequilibration, (2) oxide silicate reequilibration, and (3) intra-oxide reequilibration (Frost et al., 1988; Frost and Lindsley, 1992). The inter-oxide

TABLE 6. Microprobe Analyses of Orthopyroxene, Olivine, and Clinopyroxene from Fe-Ti Ores of the Suwalki Anorthosite

	Depth (m)	n		SiO_2	TiO_2	Al_2O_3	FeO_{tot}	MnO	MgO	CaO	Na_2O	Total	Mg #
Orthopyroxene													
K2-01	1014	5	pmih-C	52.10	0.24	2.18	18.96	0.50	23.33	1.01	-	98.32	68.7
K12-02	989	5	pmih-C	52.06	0.24	2.01	18.70	0.49	24.02	1.14	-	98.66	69.6
K12-05	1453	4	pmihc-C	51.72	0.32	1.74	20.58	0.55	22.17	1.28	-	98.36	65.8
K20-03	1611	3	pmi-C	52.19	0.28	2.20	18.56	0.46	24.18	1.09	-	98.96	69.9
K20-04	1622	3	pmi-C	52.47	0.26	2.31	17.40	0.42	24.60	0.84	-	98.30	71.6
K20-05	1721	6	pmih-C	51.63	0.32	4.03	16.28	0.30	25.59	0.59	-	98.74	73.7
K20-06	1735	8	pmi-C	52.38	0.38	4.95	14.63	0.26	26.84	0.49	-	99.93	76.6
K22-01	1717	4	pmih-C	51.86	0.33	3.28	16.80	0.36	25.23	0.73	-	98.59	72.8
K57-02	337	3	pmih-C	52.52	0.25	3.32	16.31	0.38	26.02	0.69	-	99.49	74.0
U2-01	1144	4	pmih-C	51.43	0.20	1.54	22.32	0.66	21.64	0.76	-	98.55	63.3
U2-03	1339	5	pmihca-C	51.27	0.11	1.07	23.41	1.04	20.15	1.00	-	98.05	60.5
U2-04	1397	9	pmihca-C	51.66	0.13	1.07	24.14	1.15	20.51	0.74	-	99.40	60.2
U2-06	1512	15	pmih-C	52.04	0.23	3.23	19.51	0.42	23.83	0.46	-	99.72	68.5
U4-01	1168	3	pmih-C	51.49	0.13	1.38	23.11	0.84	20.72	0.58	-	98.25	61.5
U4-02	1205	4	pmihca-C	51.63	0.10	1.09	23.92	1.26	20.42	0.80	-	99.22	60.3
U4-03	1257	5	pmih-C	52.02	0.35	1.78	19.40	0.48	23.63	1.25	-	98.91	68.5
U4-05	1379	4	pmih-C	51.56	0.23	3.16	18.57	0.40	24.29	0.49	-	98.70	70.0
U5-02	1256	5	pmih-C	51.72	0.17	1.49	21.47	0.62	22.25	0.86	-	98.58	64.9
U5-04	1373	2	pmi-C	51.96	0.28	3.25	16.70	0.34	25.37	0.61	-	98.51	73.0
J1-01	1124	18	pmih-C	52.84	0.20	1.99	19.52	0.51	23.97	0.99	-	100.02	68.6
J1-02	1240	3	pmihca-C	51.38	0.14	1.06	24.24	0.69	20.34	0.59	-	98.44	59.9
J2-01	1305	13	pmih-C	52.29	0.14	1.70	21.65	0.88	22.46	0.53	-	99.65	64.9
J2-02	1561	3	pmih-C	51.57	0.25	2.97	18.60	0.41	24.02	0.61	-	98.43	69.7
J2-03	1584	3	pmih-C	52.23	0.30	3.55	16.29	0.30	25.89	0.55	-	99.11	73.9
Olivine													
K20-03	1611	3	pmi-C	36.50	0.05	0.04	30.77	0.47	31.22	0.03	-	99.08	64.4
K20-05	1721	3	pmih-C	36.84	0.03	0.01	28.28	0.36	33.66	0.01	-	99.19	68.0
K20-06	1735	11	pmi-C	38.58	0.02	0.03	22.63	0.30	38.65	0.01	-	100.22	75.3
K22-01	1717	3	pmih-C	36.55	0.03	0.02	29.06	0.39	32.63	0.02	-	98.70	66.7
Clinopyroxene													
U2-03	1339	3	pmihca-C	50.37	0.29	2.03	9.97	0.52	12.67	21.55	0.37	97.77	69.4
U2-04	1397	9	pmihca-C	51.14	0.36	2.33	9.61	0.53	12.80	22.55	0.36	99.68	70.4
U4-02	1205	2	pmihca-C	49.51	0.63	2.03	10.56	0.51	13.17	20.72	0.40	97.53	69.0
J1-02	1240	3	pmihca-C	50.46	0.70	2.05	11.55	0.34	14.11	18.87	0.31	98.39	68.5

n = the number of microprobe analyses

TABLE 7. Whole-Rock Composition of Fe-Ti Ores from the Suwalki Anorthosite

	Depth (m)		SiO_2	TiO_2	Al_2O_3	Fe_2O_{3tot}	MgO	MnO	CaO	Na_2O	K_2O	P_2O_5	Total	Ni	V	Cr	Zn
K12-04	1060	pmih-C	23.33	7.34	9.04	49.11	7.39	0.27	3.32	0.85	0.15	0.01	100.81	384	1436	254	494
K20-03	1611	pmi-C	15.28	9.28	10.10	57.74	3.02	0.25	3.40	1.09	0.17	0.01	100.34	505	1871	335	628
K20-05	1721	pmih-C	11.03	9.48	10.02	61.80	5.15	0.22	2.14	0.52	0.08	0.01	100.45	599	2603	764	678
K20-06	1735	pmi-C	2.61	9.92	9.95	71.87	5.17	0.24	0.64	0.01	0.04	0.01	100.46	1035	3839	849	928
K20-07	1813	pmih-C	29.78	5.60	11.82	39.54	8.12	0.22	4.45	1.25	0.15	0.01	100.94	376	987	240	355
K20-08	1863	pmi-C	0.46	11.05	7.75	76.25	5.01	0.24	0.12	0.01	0.05	0.01	100.95	917	3991	958	937
K48-03	1122	pmi-C	2.95	12.96	5.83	73.59	3.69	0.29	0.77	0.01	0.04	0.01	100.14	586	3397	1758	1063
U2-02	1169	pmih-C	24.89	8.22	10.09	45.92	5.55	0.28	4.07	1.38	0.30	0.15	100.85	315	1123	264	473
U4-02	1205	pmihca-C	32.07	5.13	7.73	35.92	6.87	0.43	8.96	0.92	0.71	2.06	100.80	32	259	127	490
U4-03	1257	pmih-C	12.14	9.75	7.55	63.76	3.76	0.27	2.29	0.82	0.22	0.05	100.61	746	2362	980	708
U4-04	1330	pmih-C	4.75	11.21	6.29	71.39	3.10	0.28	1.25	1.85	0.16	0.03	100.31	717	3005	4409	1015
U4-05	1379	pmih-C	5.49	11.80	6.80	69.46	3.46	0.29	1.22	0.57	0.11	0.01	99.21	689	2859	4226	932
U4-06	1408	pmi-C	1.86	11.97	6.63	73.18	4.05	0.28	0.44	0.01	0.04	0.01	98.47	966	3320	8214	878
U5-02	1256	pmih-C	31.16	7.06	11.69	37.49	5.94	0.25	5.00	1.47	0.31	0.11	100.48	189	871	209	341
U5-04	1373	pmi-C	2.82	11.82	6.57	73.90	3.29	0.28	0.84	0.01	0.04	0.01	99.58	1018	3219	2788	959
J1-01	1124	pmih-C	14.32	9.22	8.15	60.38	4.33	0.27	2.72	0.80	0.16	0.07	100.42	707	2080	546	738
J1-02	1240	pmihca-C	41.58	4.36	14.42	22.98	5.74	0.23	7.91	2.04	0.39	0.45	100.10	21	348	121	186

Major elements in wt percent; trace elements in ppm

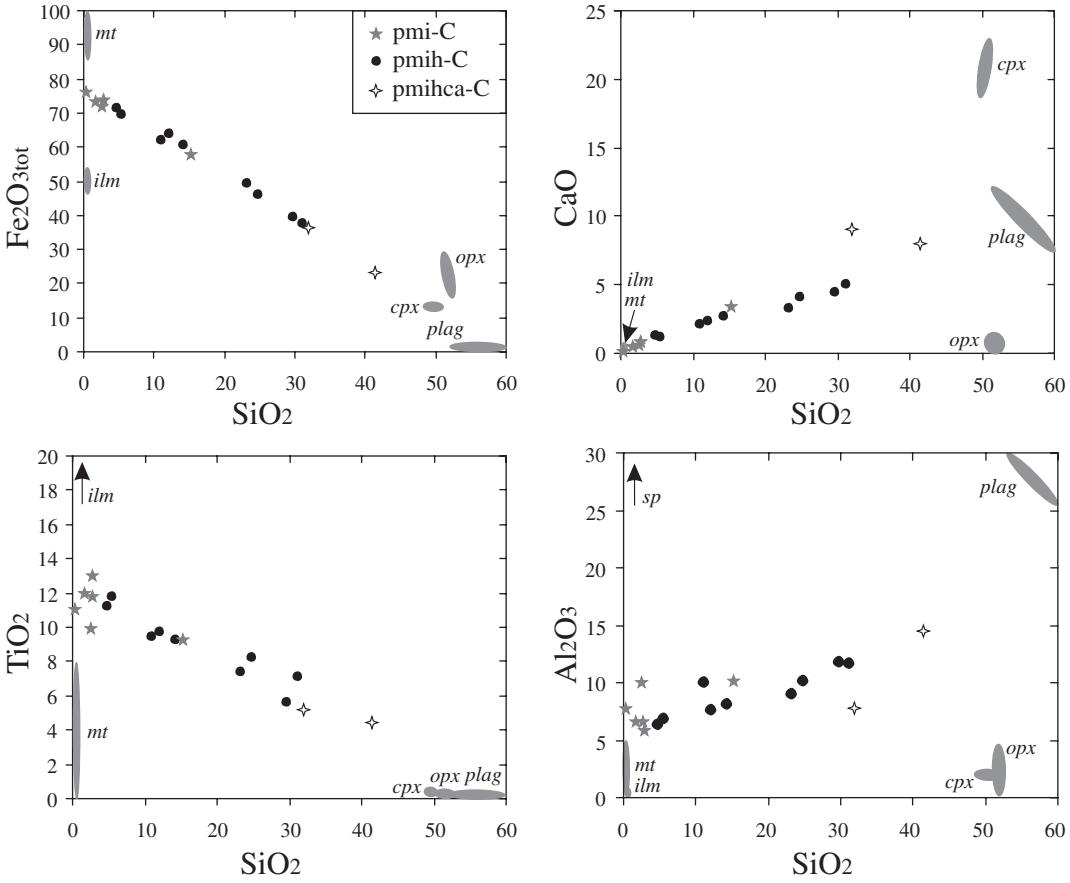

FIG. 9. Binary major elements variation diagrams of whole rocks from the Suwalki anorthosite. The compositional ranges of cumulus minerals are represented by elliptic areas or indicated by an arrow: plag = plagioclase, opx = orthopyroxene, mt = magnetite, ilm = ilmenite, cpx = clinopyroxene, sp = aluminous spinel.

reequilibration can be evaluated with the geothermometer-oxybarometer of Spencer and Lindsley (1981), which gives the T and f_{O_2} values at equilibrium between the oxides. At 3 kbar, temperatures in the 530° to 580°C range and f_{O_2} between FMQ –2.6 and FMQ +0.4 (where FMQ is the fayalite-magnetite-quartz buffer) are obtained. The same interval of values is indicated by the pyroxene-QUILF program of Andersen et al. (1993), which accounts for equilibrium of the oxides with silicates (orthopyroxene, to be specific). It can thus be determined that the last exchange of elements between the oxides and orthopyroxene has taken place in these T-f_{O_2} intervals.

Applying QUILF on the two oxides-orthopyroxene-clinopyroxene association found in sample U2-04 leads to ca. 600°C and FMQ +2. Interestingly, by allowing the Ti and Mg contents of the magnetite and the Fe^{3+} content of the ilmenite to vary, the two pyroxenes equilibrium indicates 828°C at FMQ +3.46, a magnetite slightly richer in Ti (NTi = 0.10 vs. 0.03) and Mg (NMg= 0.06 vs. 0.02) and an ilmenite richer in hematite (Xhem = 0.59 vs. 0.08).

QUILF can also be used to estimate the composition of the oxides coexisting with orthopyroxene at possible liquidus T-f_{O_2} conditions. Although the system is not sufficiently constrained

TABLE 8. Correlation Matrix for Whole-Rock Major Elements of Fe-Ti Ores from the Suwalki Anorthosite

	SiO_2	TiO_2	Al_2O_3	Fe_2O_{3tot}	MgO	MnO	CaO	Na_2O	K_2O	P_2O_5
SiO_2	1.00	–	–	–	–	–	–	–	–	–
TiO_2	–0.95	1.00	–	–	–	–	–	–	–	–
Al_2O_3	0.77	–0.79	1.00	–	–	–	–	–	–	–
Fe_2O_{3tot}	–1.00	0.95	–0.79	1.00	–	–	–	–	–	–
MgO	0.69	–0.79	0.57	–0.70	1.00	–	–	–	–	–
MnO	0.09	–0.07	–0.48	–0.09	0.02	1.00	–	–	–	–
CaO	0.94	–0.91	0.61	–0.94	0.59	0.36	1.00	–	–	–
Na_2O	0.74	–0.66	0.58	–0.73	0.27	–0.06	0.67	1.00	–	–
K_2O	0.76	–0.75	0.32	–0.76	0.43	0.63	0.92	0.57	1.00	–
P_2O_5	0.48	–0.52	0.03	–0.49	0.36	0.82	0.73	0.18	0.88	1.00

TABLE 9. Factor Loadings of the Principal Components (PC1 and PC2) for Fe-Ti Ores of the Suwalki Anorthosite

	PC1	PC2
SiO_2	–0.97	–0.16
TiO_2	0.97	0.16
Al_2O_3	–0.70	–0.65
Fe_2O_{3tot}	0.98	0.16
MgO	–0.71	–0.17
MnO	–0.24	0.96
CaO	–0.98	0.14
Na_2O	–0.71	–0.26
K_2O	–0.86	0.46
P_2O_5	–0.64	0.73
Variance	6.51	2.28
Proportion	0.65	0.23

to lead to exact solutions, the results clearly show that the primary magnetite and ilmenite were much richer in ulvöspinel and hematite, respectively, than the measured compositions after subsolidus reequilibration. This corroborates the generally observed subsolidus evolution trends of the oxides toward end-member compositions (e.g. Duchesne, 1972; Frost et al., 1988) and points to the importance of the reequilibration processes in modifying the primary liquidus compositions.

Magnetite and ilmenite contain Al_2O_3, which is ignored in the QUILF projections (Frost et al., 1988; Pang et al., 2008b). Nevertheless, in the Suwalki deposit, aluminous spinel is obviously a significant constituent of Fe-Ti oxide compositions and participates in the reequilibration processes. First, as we have deduced from the whole-rock compositions (Fig. 9), aluminous spinel grains are exsolved from the magnetite and ilmenite solid solutions as external granules (Fig. 6b). Second, aluminous spinel is also produced by oxy-exsolution, in the same way as ilmenite, in intra- and inter-oxide reequilibration. This is evidenced by the general occurrence of minute spinel grains in the (111) network of ilmenite lamellae in magnetite as well as in the rims and external granules of ilmenite at the contact with primary ilmenite (Fig. 6). Obviously, Al and Mg play crucial roles in the equilibrium between titanomagnetite and ilmenite, not only at the liquidus stage (Sauerzapf et al., 2008), but also in the subsolvus reequilibration.

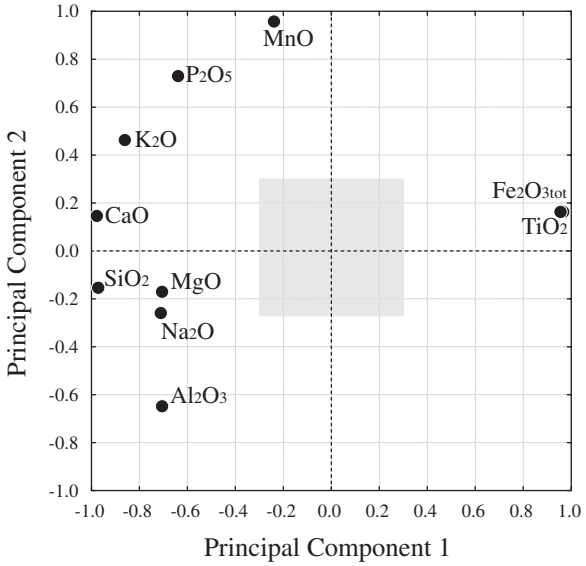

FIG. 10. Graphical representation of the factor loading in the plane of the principal components 1 and 2.

V in magnetite: further evidence for high f_{O_2}

Cr and V are usually considered as highly compatible elements in magnetite. Experiments on ferrobasalts by Toplis and Corgne (2002) have described the relation of $D_V^{mt/liq}$ and $D_{Cr}^{mt/liq}$ with f_{O_2}. In phosphorous-bearing systems, $D_{Cr}^{mt/liq}$ increases from 27 to 291 with decreasing oxygen fugacity from NNO + 2.6 to NNO–0.7 (where NNO is the nickel-nickel oxide buffer), while $D_V^{mt/liq}$ increases from 2 to 29. Consequently, even at high f_{O_2}, Cr has a bulk compatible behavior ($D_{Cr}^{bulk/liq} > 1$) as far as the cotectic proportion of magnetite is higher than 4 percent. However, for relatively high f_{O_2} and thus low $D_V^{mt/liq}$ and the same proportion of magnetite, V could behave as an incompatible element.

In Fe-Ti oxide ores of the Suwalki anorthosite, Cr in magnetite displays a large range from 6,781 to 455 ppm, whereas V in magnetite displays a smaller range from 3,773 to 6,739 ppm in pmi-C and pmih-C (Fig. 11). Similarly, V in magnetite remains constant for a large range of Mg# of orthopyroxene (77–60). Actually, the measured V content in magnetite separates is even slightly higher than the real liquidus composition due to possible exsolution of external granule of aluminous spinel. Indeed, the V content of aluminous spinel (450 ppm on average, Table 4) is about 10 times lower than the V content of magnetite (ca. 5,000 ppm, Table 2) and its exsolution is responsible for the relative enrichment of magnetite. The V content of liquidus magnetite is thus actually located on the tie line between aluminous spinel and reequilibrated magnetite (Fig. 11), with the precise location depending on the proportion of aluminous spinel exsolved as external granules. The Cr content of magnetite is negligibly influenced by the exsolution of aluminous spinel because it is only slightly Cr richer than magnetite.

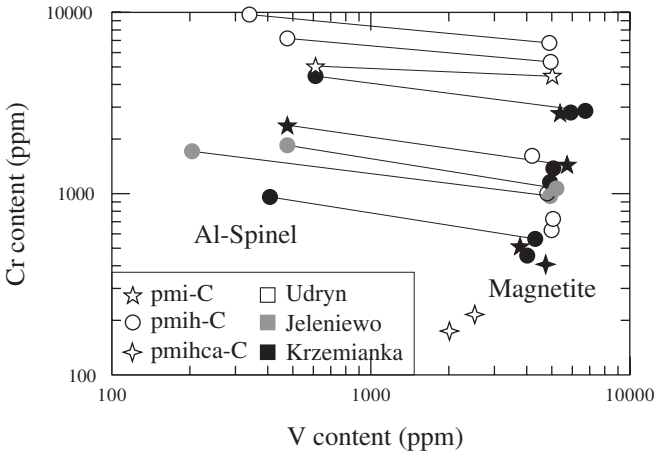

FIG. 11. Cr (ppm log unit) as a function of V (ppm log unit) in magnetite and aluminous spinel from Fe-Ti oxide ores in the Suwalki anorthosite. Different symbols are used to discriminate the mineral assemblages and different grays, the occurrences.

The constant V content in magnetite implies a $D_V^{bulk/liq}$ around 1 in pmi-C and pmih-C and thus a relatively low $D_V^{mt/liq}$, which is interpreted to result from a relatively high f_{O_2} in primitive cumulates. This results from the high proportion of V^{4+} and V^{5+} valences at high f_{O_2}, which are less partitioned in magnetite compared to V^{3+} (Toplis and Corgne, 2002). The high f_{O_2} is thus also responsible for the relatively low V content in magnetite from Fe-Ti oxide ores in the Suwalki anorthosite (0.37–0.67 wt % V) compared to the Bushveld complex where it reaches 1.3 percent V at the base of the magnetite layers (Cawthorn and Molyneux, 1986; Tegner et al., 2006) or the Fedorivka layered intrusion (up to 1.85 wt % V; Duchesne et al., 2006). V in magnetite starts decreasing significantly in more evolved cumulates in which clinopyroxene ± apatite are liquidus phases. This is interpreted to result from a decreasing f_{O_2} with differentiation.

Polybaric Crystallization and Fractionation Trends

Classical views on the emplacement mechanism of Proterozoic massif-type anorthosites involve polybaric crystallization, starting at about 10 to 13 kbar up to the final depth of emplacement between 3 to 5 kbar (e.g., Ashwal, 1993; Longhi et al., 1993). Buoyant plagioclase cumulates that formed in a deep-seated magma chamber intrude the middle to upper crust by diapirism (Barnichon et al., 1999), probably channeled by zones of weakness (Scoates and Chamberlain, 1997; Duchesne et al., 1999) owing to gravitational instabilities. Parental and residual liquids are swept along with the anorthositic mush to crystallize over a large pressure interval (Longhi et al., 1993). According to the experiments of Longhi et al. (1993), the occurrence of high-alumina orthopyroxene megacrysts in the Suwalki anorthosite (Wiszniewska et al., 2002) is evidence of high pressure crystallization at 10 to 13 kbar.

This dynamic and polybaric crystallization of massif-type anorthosites may have a significant influence on the mechanisms of formation of Fe-Ti oxide ores in the Suwalki anorthosite. Several observations suggest that these oxide ores have crystallized continuously during the rising of the anorthosite diapir.

Polybaric crystallization and fractionation trends: Insights from Al_2O_3 in orthopyroxene and Cr in magnetite

Experiments by Longhi et al. (1993) have demonstrated that the Al_2O_3 partitioning between orthopyroxene and plagioclase-saturated liquid is directly correlated with the pressure of crystallization, and to a lesser extent with the temperature of crystallization. Other compositional controls have relatively minor effects. In Fe-Ti ores of Suwalki anorthosite, Al_2O_3 in orthopyroxene varies from 4.95 to 1.06 wt % (Table 6), the composition in a single sample being highly constant. It is also obvious from Figure 8d that the Al_2O_3 content of orthopyroxene displays significant scattering at the same Mg#, particularly for the most primitive samples (higher Mg#). This large range of orthopyroxene composition may be explained by variable pressures of crystallization of the different rocks, which tend to decrease with differentiation. It is worth noting that Wiszniewska et al. (2002) have described high-alumina orthopyroxene megacrysts in the Suwalki anorthosite. These orthopyroxenes host plagioclase lamellae, testifying to originally higher Al_2O_3 content, and thus higher maximum pressure of crystallization for the anorthosite pluton. However, without a calibration of the Al_2O_3 content in orthopyroxene as a barometer, it is rather uncertain how much decompression has occurred.

It is also obvious from the two trends of Figure 12a and b that samples from Udryn deposit on one hand and samples from Jeleniewo and Krzemianka deposits on the other hand are clearly discriminated in the plots of Al_2O_3 and Mg# of orthopyroxene as a function of Cr in magnetite, considered as a differentiation index. Because the partitioning of Mg between orthopyroxene and melt is not correlated with the pressure of crystallization (Fram and Longhi, 1992; Vander Auwera and Longhi, 1994; Longhi et al., 1999), the discrimination between the two groups may only result from variable contents of Cr in magnetite. Two hypotheses may be proposed: (1) different Cr compositions of the parental magma and/or, (2) different f_{O_2} of crystallization, responsible for variable $D_{Cr}^{mt/liq}$ (see discussion on V in magnetite). Because of extensive subsolidus reequilibration of Fe-Ti oxides and thus the inability of the QUILF equilibria to give accurate high-temperature magmatic f_{O_2}, the solution might come from a study of the Cr

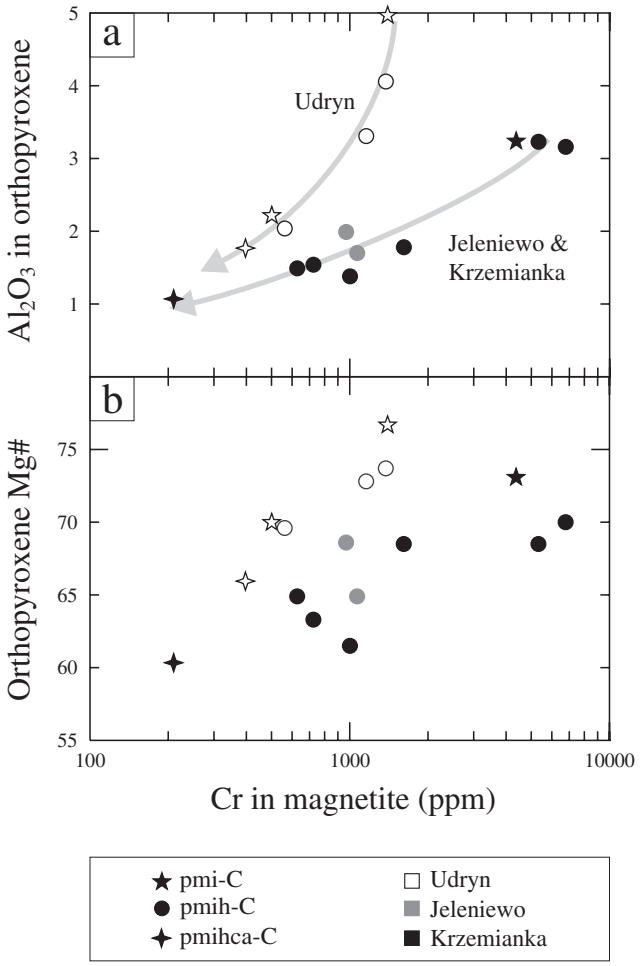

FIG. 12. a. Al_2O_3 content (wt %), and b. Mg# of orthopyroxene (molar %) as a function of Cr in magnetite (ppm log unit). Gray arrows indicate the differentiation paths of the different occurrences.

content in orthopyroxene (not sensitive to variable f_{O_2}) in high-pressure plagioclase-orthopyroxene assemblages (before Fe-Ti oxides fractionation).

It emerges from Figure 12 that two differentiation trends occur in Fe-Ti oxide ores. This seems contradictory with their crystallization in the single Suwalki anorthosite, most probably from residual melts of the anorthosite pluton. However, the 80 km² anorthosite body is only known from drill cores. It would thus not be surprising that the Suwalki anorthosite is actually a composite intrusion made up of several smaller anorthosite diapirs. It is remarkable that the Sr and Ba contents of plagioclase (Fig. 8b) also discriminate the Udryn from the Krzemianka deposits. This may indicate that different compositions of parental magma are involved in the formation of the Suwalki anorthosite. Diversity among primitive magmas in a single anorthosite province has already been evidenced by Bolle et al. (2003) in Norway. It is interpreted to result from partial melting of variable mafic lower crust components (Schiellerup et al., 2000; Longhi, 2005).

Implications of the polybaric crystallization on the stability fields of orthopyroxene and Fe-Ti oxides

Using the MELTS algorithm of Ghiorso and Sack (1995) to assess the liquidus assemblage of ferrodiorites and inversion of plagioclase composition using partition coefficients between plagioclase and melt, Wiszniewska et al. (2002) have identified fine-grained ferrodiorites as parental magma to the Suwalki anorthosites. Experimental liquidus phases of similar liquid compositions, which represent plausible parent magmas of massif-type anorthosite, are initially saturated in plagioclase + orthopyroxene at pressure >5 kbar (Fram and Longhi, 1992; Vander Auwera et al., 1998; Longhi et al., 1999). This is illustrated in the Suwalki anorthosite by the occurrence of high-alumina orthopyroxene with plagioclase megacrysts (Wiszniewska et al., 2002). However, in Fe-Ti oxide-rich rocks of Suwalki, plagioclase may occur with magnetite and ilmenite alone, without orthopyroxene.

Even if this has not been clearly shown in ferrobasaltic systems, it is most probable that the temperature-pressure slope for the orthopyroxene liquidus is much steeper than that for Fe-Ti oxides (ilmenite and magnetite) liquidus. This has been shown for the ilmenite liquidus by the experiments of Delano (1980) on phase relations of high-Ti mare basalts. The occurrence of different cumulus assemblages may thus result from different pressures of crystallization. Whereas the assemblage plagioclase + high-alumina orthopyroxene crystallizes at high pressures (13–10 kbar), the assemblage plagioclase + magnetite + ilmenite may crystallize at lower pressures (8–5 kbar) from the same parental magma. Such phase equilibria could occur for ferrodioritic compositions such as the TJ-liquid of Vander Auwera et al. (1998) and Longhi et al. (1999) but with slightly higher FeO and TiO_2 contents.

Conclusions

Fe-Ti-rich rocks responsible for gravimetric and magnetic anomalies in the Suwalki anorthosite and intersected by drill cores at 820- to 2,600 m depth are closely related to the emplacement of the anorthosite pluton and do not represent isolated magma chambers. These rocks are cumulates and the different parageneses are related by a fractional crystallization process. Parental ferrodioritic magma of anorthosite, initially saturated in plagioclase + orthopyroxene at high pressures, is saturated in plagioclase + magnetite + ilmenite at the pressure of crystallization of Fe-Ti oxide ores. The magma was then saturated in orthopyroxene, followed by clinopyroxene, and, finally, apatite. Crystal sorting of Fe-Ti oxides relative to plagioclase and ferromagnesian silicates is responsible for the formation of oxide-enriched layers. This sorting was favored by the dynamic and diapiric uprising of the anorthosite pluton during the crystallization of Fe-Ti-enriched cumulates, as shown by polybaric evidence such as variable Al_2O_3 content in orthopyroxene. Individual differentiation trends indicate that different parental magmas may have been involved and thus that the Suwalki anorthosite may be a composite pluton. In contrast to exploited Fe-Ti oxide deposits (Tellnes and Lac Tio), cumulates from the Suwalki anorthosite are dominated by magnetite with minor ilmenite. The crystallization of magnetite is further supported by high f_{O_2} conditions, inferred from the low and constant V content in magnetite.

Fe-Ti oxide-rich rocks from Suwalki represent very large mineral resources of a particular ore type associated with Proterozoic anorthosites, dominated by V-poor Ti magnetite. These Fe-Ti deposits are significant in terms of tonnage and are primarily iron deposits, with by-product options for titanium and vanadium. However, the Suwalki Fe-Ti ores are not presently economic due to the depth of the orebodies and the fact that such ores are not easily processed and refined. However, the Suwalki deposits represent major future mineral resources for Europe, depending on developments in underground mining, mineral processing, and the value of iron.

Acknowledgments

This work was funded by the Belgian Fund for Joint Research and the Fund for Research in Industry and Agriculture. Fieldwork was supported by the Commission Générale pour les Relations Internationales de la Communauté française de Belgique and BC has benefited from a student research grant from the Society for Economic Geologists. The Polish Geological Institute is thanked for its hospitality and for giving access to the samples. Caroline-Emmanuelle Morisset, Anne Bouton, and Are Korneliussen are greatly acknowledged for assistance in fieldwork, samples preparation, and SEM pictures, respectively. Comments by Peter Lightfoot on an early version have been helpful. Larry Meinert is acknowledged for his editorial handling. This paper has benefited from constructive reviews by Are Korneliussen, James Scoates, and Christian Tegner.

August 7, 2008; February 19, 2009

REFERENCES

Andersen, D.J., Lindsley, D.H., and Davidson, P.M., 1993, QUILF: A PASCAL program to assess equilibria among Fe-Mg-Ti oxides, pyroxenes, olivine, and quartz: Computers in Geosciences, v. 19, p. 1333–1350.

Ashwal, L.D., 1993, Anorthosites: Heidelberg, Springer, 422 p.

Baginski, B., Duchesne, J.-C., Vander Auwera, J., Martin, H., and Wiszniewska, J., 2001, Petrology and geochemistry of rapakivi-type granites from the crystalline basement of the NE Poland: Geological Quarterly, v. 45, p. 33–52.

Barnichon, J.-D., Havenith, H., Hoffer, B., Charlier, R., Jongmans, D., and Duchesne, J.C., 1999, The deformation of the Egersund Ogna massif, South Norway: Finite element modelling of diapirism: Tectonophysics, v. 303, p. 109–130.

Bateman, A.M., 1951, The formation of late magmatic oxide ores: Economic Geology, v. 46, p. 404–426.

Bogdanova, S.V., Page, L.M., Skridlaite, G., and Taran, L.N., 2001, Proterozoic tectonothermal history in the western part of the East European craton: $^{40}Ar/^{39}Ar$ geochronological constraints: Tectonophysics, v. 339, p. 39–66.

Bogdanova, S.V., Bingen, B., Gorbatschev, R., Kheraskova, T.N., Kozlov, V.I., Puchkov, V.N., and Volozh, Y.A., 2008, The East European craton (Baltica) before and during the assembly of Rodinia: Precambrian Research, v. 160, p. 23–45.

Bolle, O., Demaiffe, D., and Duchesne, J.C., 2003, Petrogenesis of jotunitic and acidic members of an AMC suite (Rogaland anorthosite province, SW Norway): A Sr and Nd isotopic assessment: Precambrian Research, v. 124, p. 185–214.

Bologne, G., and Duchesne, J.C., 1991, Analyse des roches silicatées par spectrométrie de fluorescence X: précision et exactitude: Geological Survey of Belgium, Professional Paper, v. 249, p. 1–11.

Cawthorn, R.G., and Molyneux, T.G., 1986, Vanadiferous magnetite deposits of the Bushveld Complex, *in* Anhaeusser, C. R., and Maske, S., eds., Mineral Deposits of Southern Africa: Geological Society of South Africa, p. 1251–1266.

Charlier, B., Duchesne, J.-C., and Vander Auwera, J., 2006, Magma chamber processes in the Tellnes ilmenite deposit (Rogaland Anorthosite Province, SW Norway) and the formation of Fe-Ti ores in massif-type anorthosites: Chemical Geology, v. 234, p. 264–290.

Charlier, B., Skår, Ø., Korneliussen, A., Duchesne, J.-C., and Vander Auwera, J., 2007, Ilmenite composition in the Tellnes Fe-Ti deposit, SW Norway: Fractional crystallization, postcumulus evolution and ilmenite-zircon relation: Contributions to Mineralogy and Petrology, v. 154, p. 119–134.

Charlier, B., Sakoma, E., Sauvé, M., Stanaway, K., Vander Auwera, J., and Duchesne, J.-C., 2008, The Grader layered intrusion (Havre-Saint-Pierre Anorthosite, Quebec) and genesis of nelsonite and other Fe-Ti-P ores: Lithos, v. 101, p. 359–378.

Ciesla, E., and Wybraniec, S., 1998, Geophysical studies of the Suwalki anorthosite massif, *in* Ryka, W., and Podemski, M., eds., Geology of the Suwalki anorthosite massif (northeastern Poland): Warsaw, Poland, Prace Panstwowego Instytutu Geologicznego, p. 27–38.

Claesson, S., Bogdanova, S.V., Bibikova, E.V., and Gorbatschev, R., 2001, Isotopic evidence for Palaeoproterozoic accretion in the basement of the East European craton: Tectonophysics, v. 339, p. 1–18.

Delano, J.W., 1980, Chemistry and liquidus phase relations of Apollo 15 red glass Implications for the deep lunar interior: Lunar and Planetary Science Conference 11th, Houston, Texas, New York, Pergamon Press, Proceedings, v. 1, p. 251–288.

Dörr, W., Belka, Z., Marheine, D., Schastok, J., Valverde-Vaquero, P., and Wiszniewska, J., 2002, U-Pb and Ar-Ar geochronology of anorogenic granite magmatism of the Mazury complex, NE Poland: Precambrian Research, v. 119, p. 101–120.

Duchesne, J.C., 1972, Iron-titanium oxide minerals in the Bjerkrem-Sogndal Massif, South-western Norway: Journal of Petrology, v. 13, p. 57-81.

——1996, Liquid ilmenite or liquidus ilmenite: A comment on the nature of ilmenite vein deposits, *in* Demaiffe, D., ed., Petrology and geochemistry of magmatic suites of rocks in the continental and oceanic crusts. A volume dedicated to Professor Jean Michot: Université Libre de Bruxelles, Royal Museum for Central Africa (Tervuren), p. 73–82.

——1999, Fe-Ti deposits in Rogaland anorthosites (South Norway): Geochemical characteristics and problems of interpretation: Mineralium Deposita, v. 34, p. 182–198.

Duchesne, J.C., and Bologne, G., 2009, XRF major and trace element determination in Fe-Ti oxide minerals. Geologica Belgica, v. 12, p. 205–212.

Duchesne, J.C., Liégeois, J.P., Vander Auwera, J., and Longhi, J., 1999, The crustal tongue melting model and the origin of massive anorthosites: Terra Nova, v. 11, p. 100–105.

Duchesne, J.C., Shumlyanskyy, L., and Charlier, B., 2006, The Fedorivka layered intrusion (Korosten Pluton, Ukraine): An example of highly differentiated ferrobasaltic evolution: Lithos, v. 89, p. 353–376.

Emslie, R.F., 1980, Geology and petrology of the Harp Lake Complex, central Labrador: an example of Elsonian magmatism: Geological Survey of Canada Bulletin, v. 293, p. 1–136.

Force, E.R., 1991, Geology of titanium-mineral deposits, U.S. Geological Survey Special Paper, 259, 112 p.

Fram, M., and Longhi, J., 1992, Phase equilibria of dikes associated with Proterozoic anorthosite complexes: American Mineralogist, v. 77, p. 605–616.

Frost, B.R., and Lindsley, D.H., 1992, Equilibria among Fe-Ti oxides, pyroxenes, olivine, and quartz: Part II. Application: American Mineralogist, v. 77, p. 1004–1020.

Frost, B.R., Lindsley, D.H., and Andersen, D.J., 1988, Fe-Ti oxide-silicate equilibria: Assemblages with fayalitic olivine: American Mineralogist, v. 73, p. 727–740.

Ghiorso, M.S., and Sack, R.O., 1995, Chemical mass transfer in magmatic processes IV. A revised and internally consistent thermodynamic model for the interpolation and extrapolation of liquid-solid equilibria in magmatic systems at elevated temperatures and pressures: Contributions to Mineralogy and Petrology, v. 119, p. 197–212.

Irvine, T.N., 1982, Terminology for layered intrusions: Journal of Petrology, v. 23, p. 127–162.

Juskowiak, O., 1998, Occurrence, structure and mineral diversity of rocks from the Suwalki anorthosite massif, *in* Ryka, W., and Podemski, M., eds., Geology of the Suwalki anorthosite massif (northeastern Poland): Warsaw, Poland, Prace Panstwowego Instytutu Geologicznego, p. 53–80.

Kolker, A., 1982, Mineralogy and geochemistry of Fe-Ti oxide and apatite (nelsonite) deposits and evaluation of the liquid immiscibility hypothesis: Economic Geology, v. 77, p. 1146–1148.

Lafrance, B., John, B.E., and Scoates, J.S., 1996, Syn-emplacement recrystallization and deformation microstructures in the Poe Mountain anorthosite, Wyoming: Contributions to Mineralogy and Petrology, v. 122, p. 431–440.

Lister, G.F., 1966, The composition and origin of selected iron-titanium deposits: Economic Geology, v. 61, p. 275–310.

Longhi, J., 2005, A mantle or mafic crustal source for Proterozoic anorthosites?: Lithos, v. 83, p. 183–198.

Longhi, J., Vander Auwera, J., Fram, M., and Monthieth, J.N., 1993, Pressure effects, kinetics and rheology of anorthositic and related magmas: American Mineralogist, v. 78, p. 1016–1030.

Longhi, J., Vander Auwera, J., Fram, M.S., and Duchesne, J.C., 1999, Some phase equilibrium constraints on the origin of Proterozoic (massif) anorthosites and related rocks: Journal of Petrology, v. 40, p. 339–362.

Morgan, J.W., Stein, H.J., Hannah, J.L., Markey, R.J., and Wiszniewska, J., 2000, Re-Os study of Fe-Ti-V oxide and Fe-Cu-Ni sulfide deposits, Suwalki anorthosite massif, northeast Poland: Mineralium Deposita, v. 35, p. 39–401.

Namur, O., Hatert, F., Grandjean, F., Long, G. J., Krins, N., Fransolet, A. M., Vander Auwera, J., and Charlier, B., 2009, Ti substitution mechanisms in phlogopites from the Suwalki massif-type anorthosite, NE Poland: European Journal of Mineralogy, v. 21, in press.

Pang, K.-N., Li, C., Zhou, M.-F., and Ripley, E., 2008a, Abundant Fe-Ti oxide inclusions in olivine from the Panzhihua and Hongge layered intrusions, SW China: Evidence for early saturation of Fe-Ti oxides in ferrobasaltic magma: Contributions to Mineralogy and Petrology, v. 156, p. 307–321.

Pang, K.-N., Zhou, M.-F., Lindsley, D., Zhao, D. and Malpas, J., 2008b, Origin of Fe-Ti oxide ores in mafic intrusions: Evidence from the Panzhihua intrusion, SW China: Journal of Petrology, v. 49, p. 295–313.

Parecki, A., 1998, Geological structure of the Krzemianka and Udryn deposits, *in* Ryka, W., and Podemski, M., eds., Geology of the Suwalki anorthosite massif (northeastern Poland): Warsaw, Poland, Prace Panstwowego Instytutu Geologicznego, p. 123–135.

Philpotts, A.R., 1967, Origin of certain iron-titanium oxide and apatite rocks: Economic Geology, v. 62, p. 303–315.

Podemski, M., 1998, Discovery and exploration of the Suwalki anorthosite massif; a case study, *in* Ryka, W., and Podemski, M., eds., Geology of the Suwalki anorthosite massif (northeastern Poland): Warsaw, Poland, Prace Panstwowego Instytutu Geologicznego, p. 7–18.

Robinson, P., Kullerud, K., Tegner, C., Robins, B., and McEnroe, S. A., 2003, Could the Tellnes ilmenite deposit have been produced by in-situ magma mixing?: Norges Geologiske Undersøkelse Special Publication, v. 9, p. 107–108.

Ryka, W., and Podemski, M., 1998, Geology of the Suwalki anorthosite massif (northeastern Poland): Warsaw, Poland, Prace Panstwowego Instytutu Geologicznego, 193 p.

Sauerzapf, U., Lattard, D., Burchard, M., and Engelmann, R., 2008, The titanomagnetite-ilmenite equilibrium: New experimental data and thermooxybarometric application to the crystallization of basic to intermediate rocks: Journal of Petrology, v. 49, p. 1161–1185.

Schiellerup, H., Lambert, D.D., Prestvik, T., Robins, B., McBride, J.S., and Larsen, R.B., 2000, Re-Os isotopic evidence for a lower crustal origin of massif-type anorthosites: Nature, v. 405, p. 781–784.

Scoates, J.S., and Chamberlain, K.R., 1997, Orogenic to post-orogenic origin for the 1.76 Ga Horse Creek anorthosite complex, Wyoming, USA: Journal of Geology, v. 105, p. 331–343.

Skridlaite, G., Wiszniewska, J., and Duchesne, J.-C., 2003, Ferro-potassic A-type granites and related rocks in NE Poland and S Lithuania: west of the East European craton: Precambrian Research, v. 124, p. 305–326.

Skridlaite, G., Whitehouse, M., and Rimsa, A., 2007, Evidence for a pulse of 1.45 Ga anorthosite-mangerite-charnockite-granite (AMCG) plutonism in Lithuania: implications for the Mesoproterozoic evolution of the East European Craton: Terra Nova, v. 19, p. 294–301.

Speczik, S., Wiszniewska, J., and Diedel, R., 1988, Minerals, exsolution features and geochemistry of Fe-Ti ores of the Suwalki district (north-east Poland): Mineralium Deposita, v. 23, p. 200–210.

Spencer, K.J., and Lindsley, D.H., 1981, A solution model for coexisting iron-titanium oxides: American Mineralogist, v. 66, p. 1189–1201.

Tegner, C., Cawthorn, R.G., and Kruger, F.J., 2006, Cyclicity in the Main and Upper zones of the Bushveld Complex, South Africa: Crystallization from a zoned magma sheet: Journal of Petrology, v. 47, p. 2257–2279.

Toplis, M.J., and Corgne, A., 2002, An experimental study of element partitioning between magnetite, clinopyroxene and iron-bearing silicate liquids with particular emphasis on vanadium: Contributions to Mineralogy and Petrology, v. 144, p. 22–37.

Vander Auwera, J., and Longhi, J., 1994, Experimental study of a jotunite (hypersthene monzodiorite): Constraints on the parent magma composition and crystallization conditions (*P, T,* f_{O2}) of the Bjerkreim-Sokndal layered intrusion (Norway): Contributions to Mineralogy and Petrology, v. 118, p. 60–78.

Vander Auwera, J., Longhi, J., and Duchesne, J.C., 1998, A liquid line of descent of the jotunite (hypersthene monzodiorite) suite: Journal of Petrology, v. 39, p. 439–468.

Wiszniewska, J., Claesson, S., Stein, H.J., Vander Auwera, J., and Duchesne, J.C., 2002, The north-eastern Polish anorthosite massifs: petrological, geochemical and isotopic evidence for a crustal derivation: Terra Nova, v. 14, p. 1–10.

Zhou, M.-F., Robinson, P.T., Lesher, C.M., Keays, R.R., Zhang, C.-J., and Malpas, J., 2005, Geochemistry, petrogenesis and metallogenesis of the Panzhihua gabbroic layered intrusion and associated Fe-Ti-V oxide deposits, Sichuan province, SW China: Journal of Petrology, v. 46, p. 2253–2280.